THE ELECTROCHEMICAL STUDIES ON BINARY OXIDE MELTS

by SEICHI SATO

ACKNOWLEDGEMENTS

I am greatly indebted to Professor T. Yokokawa for many helpful suggestions and discussions relating to this work.

I am glad to acknowledge the helpful suggestions I have accepted from Professor H. Kita especially with respect to electrochemistry.

Further, I would like to thank Professor M. Shimoji for critically reading the entire manuscript and making many helpful suggestions.

I am grateful to Mrs. S. Narita and my wife, for the assistance in preparing this manuscript.

CONTENTS

I INTRODUCTION

I-1 The Purpose of the Present Study

Molten oxide mixtures floating on molten metals are of great use in iron manufacture, steelmaking process and extraction metallurgy as the materials for thermal isolation between gas phase and molten metals and as the substances contributing to mass transfer and exchange reaction with molten metals. They have also been used as enamels in ceramics for a long time. Here molten oxide mixtures consist of acidic oxide, SiO_2, GeO_2, B_2O_3, P_2O_5 on one hand and of various metallic oxides of basicity on the other hand. Up to now a considerable amount of experiments has been devoted to the studies of the oxide melts including SiO_2, in the composition ranges of high metallic oxides.

On the other hand, from the point of scientific view, we are more interested in these oxide mixtures in the region of the high concentration of acidic oxide. Acidic oxides form three dimentional net-work structure in liquid state. When the metallic oxides are added to them, the net-works are modified locally and the three dimentional polymers gradually change into fragments of various sizes depending on the amount of metallic oxides. Corresponding to this, conductivity and

fluidity increase from extremely small to large value and the liquids become ionic with so called fused salt nature. These behaviors seem to be characteristic to oxide systems which melt at high temperature and cannot be found in other solutions, like aqueous solutions, organic and polymer solutions etc. They are also different from typical fused salt mixtures.

To clearify the nature of these mixtures as solution, the kinetic and thermodynamic as well as spectroscopic data are indispensable. Spectroscopic measurements are too difficult or impossible regretfully in spite of the advantage of its direct method. Kinetic method have been carried out with respect to the viscosities and electric conductivities. Though the partial thermodynamic quantities, $\Delta\overline{S}$, $\Delta\overline{H}$ and $\Delta\overline{G}$ are important and indispensable, they are known only partially, especially in acidic oxide-rich composition. Vapor pressure and chemical equilibrium measurements at high temperature are not appropriate, for such kind of studies usually give the poor accuracy. Emf measurement with formation cells are also not appropriate because of severe contamination of alumina crucible at the metal-melt interface.

In this article the present author studied the oxygen electrode reaction at noble metal-melt interface at equilibrium with oxygen by means of electromotive

force measurements to clearify what electrode reaction is potential determining and studied kinetic processes of the electrode reaction by electrolysis with stabilized zirconia as electrode constituent. By using the electrode reaction which has now clearly defined as mentioned above, the thermodynamic quantities $\Delta\overline{G}$ $\Delta\overline{H}$ $\Delta\overline{S}$ of the respective component in molten binary oxide mixtures, Li_2O-B_2O_3, Na_2O-B_2O_3, K_2O-B_2O_3 systems were determined in acidic oxide-rich composition. The same technique was applied to Na_2O-P_2O_5 system. The data are discussed with other physco-chemical properties and compared with those of other solutions.

I-2 The Historical Review of the Studies on Oxide Mixtures

Phase diagrams in ceramics have been studied for a long time. At the beginning of 1930s, two handred phase diagrams have already been reported. In solid state, many stoichiometric compounds are found in binary or ternary oxide system. In a period of the story it has been considered that the compounds of the stoichiometries are stable in liquid phase and such a neutral compounds can react chemically each other in bulk or across phase boundary. In such a case, structure and constitution of molten oxide mixtures need not be discussed further.

But later, the melts were brought to structural study which was aided by the development of experimental methods and of the theories of aqueous solutions. The works were initiated firstly by Endell and Hellbrugge with respect to viscous flow[1]. After 1952, Shartsis et al.[2] and Bockris et al.[3] measured conductivities, viscosities, densities and expansivities for silicate melts. Especially Bockris et al. proposed some models of ionic species corresponding to the particular compositions in the range of metallic oxide less than 55 mol %, which is now called discrete anion model[3]. In consequence of these experiments, it has become clear that oxide mixtures are belong to a kind of dissociated electrolytic solutions*, like fused alkali halide.

* The electric conductivities of the melts below 15 mol % in metallic oxide could not be measured[4], owing to the high melting temperatures and corrosion of molybdenum crucible used as the cell.

The methods which are considered to be more direct for research of the structure of a solution like X-ray analysis, n.m.r., I.R., Raman and microwave absorption, are too difficult or impossible to be applied because of high temperature. The kinetic methods are considered to be practical and applicable at high temperature. Thus Shartsis et al.[5,6] and Riebling et al.[7,8] have studied electric conductivities and viscosities of borates and germanates, respectively. The liquidus for these systems are sufficiently lower than melting point of Pt and the data can be obtained even in the dilute solution of metallic oxide below 0.01 mol fraction with Pt assembly.

By X-ray diffraction studies of Warren and co-workers[9] from 1934, it became clear that silicate glasses from pure silica to meta-silicate composition form three dimentional random net-works, which are called Zachariasen-Warren random net-work model. In the oxide mixtures, it has been shown that the random net-works are also retained in SiO_2 rich composition, as is exemplified by the high value of viscosities. The same situations are also realized in germanates, borates and phosphates.

For molten oxide mixtures the both two models are acceptable. Thus, in a basic composition, say, 0.5 or higher by mole fraction of a metallic oxide, the discrete anion model is real and in the other composition the random net-work model is appropriate.

Since oxide mixtures have obviously been regarded as a ionic liquid, thermodynamic activities of the components, interfacial phenomena, and transport phenomena have been tried electrochemically. The leading and excellent study has been carried out by King and Ramachandran[10] who showed how the components transfer with electrode potential through a interface between two liquids of an alloy and an oxide mixture. But the electrochemical method which is very convenient at room-temperature have some decisive difficulties at high temperature. Since oxide mixtures are so-called concentrated solution, we can not prepare the reference cell which can be well-definied in common with many different melts. The control of the concentration of substances in a mixture are difficult because of the large exchange reaction with atmosphere or with the container, for example oxygen. Exchange electrode reactions are also very rapid. We can not obtain appropriate insulator endurable at high temperature etc. Owing to such problems, it is very difficult to determine what electrode reaction determines

the potential and what electrode process occurs, although recently the transient methods at short intervals from m-sec to μ-sec order have given promise of the analysis. In spite of this, up to now, many thermodynamic activities of the components in oxide mixtures have been reported[11] by emf method where it was assumed that such-and-such reaction determined the emf and such-and-such ion exclusively carry the current. Because of the contamination from alumina as a container etc, data of various authors do not always coincide and there are only a few cases where $\Delta\bar{H}$ and $\Delta\bar{S}$ are reported. Other many activity measurements also have been carried out by means of a chemical reaction[11], cryoscopy[12~15] (from phase diagram), solubility[16~18], and measurements of vapor pressure[19,20] by thermoblance or mass-spectrometer.

These many activity of these mixtures have demanded the explanation. From 1962, Toop et al.[21] Masson et al.[22,23] Yokokawa et al.[24,25] and Frohberg et al.[26] treated these data by assuming an unvariable equilibrium constant over wide composition range with respect to reaction of the net-work modification

$$O^{2-} + \gtrless Si\text{-}O\text{-}Si \lesssim \rightleftharpoons 2 \gtrless SiO^{-}.$$

The activities are explained by the assumption that the configurational entropy arising from net-work modification

determines the behavior of activity with composition. In such a manner of progresses a role of calorimetry in this field can not be neglected. Kleppa et al. developed the high temperature calorimeter which could be used up to 1000°C. Since 1964, they have measured enthalpies of mixing and/or relative partial molar enthalpies in binary oxide mixtures, namely vanadate[27], molybdate[28], borate[29], silicate[30] and alkali-fluoride beryllium fluorid mixtures[31]. From the view point of a solution, the relative partial molar enthalpies are one of the very important quantities in relation to the structual properties of a solution, especially when we see only the free energies have been known so far and when we face the difficulties of spectroscopic methods at high temperature.

In the present section, the developments of oxide mixtures have traced. The recent advances are remarkable and many methods have been applied. However, there are many problems to be resolved more clearly such as the ionic state in solution, especially the anionic structure, acidity and basicity, the structure of coordinated ion, appearence of two immiscible liquid phases, the relation between viscosity and conductivity, transport phenomena and electrode kinetics etc.

I-3 Outline of this Study

I-3-1 Oxygen Electrode Reaction

In 1940, Dietzel and his co-workers[32,33] firstly analysed the electrode reaction of the electrode system, $(Pt)O_2|$alkali oxide melt, as follows

$$O^{2-} \rightleftharpoons \frac{1}{2} O_2 + 2e.$$

The reaction was concluded to determine the potential, after they compared the emf value with theoretical one corresponding to oxygen pressure difference using the oxide melt as electrolyte. Later, Førland et al.[34] criticized their treatment because it is not definite as yet what chemical species determine the potential with oxygen. After 1957, calcia-stabilized Zirconia, $ZrO_2(CaO)$ has been developed as a solid electrolyte whose sole carrier is O^{2-} ion[35]. Many thermodynamic data for free energy of formation with respect to oxides or alloys at high temperature have been obtained by means of the solid electrolyte. The present author made use of this solid electrolyte as electrode constituent in stead of electrolyte in the following cell[36].

$$(Pt)O_2 \mid ZrO_2(CaO) \mid Na_2O\text{-}B_2O_3(I) \parallel Na_2O\text{-}B_2O_3(II) \mid ZrO_2(CaO) \mid O_2(Pt) \quad i)$$

$$(Pt)O_2 \mid Na_2O\text{-}B_2O_3(I) \parallel Na_2O\text{-}B_2O_3(II) \mid O_2(Pt) \quad ii)$$

The emf values between two cells agreed very much with each other. This result proves the oxygen electrode reaction to determine the Pt-electrode potential at equilibrium.

Further, the electrolysis in $Na_2O\text{-}B_2O_3$ or $Na_2O\text{-}SiO_2$ melt was carried out in stationary state[37] in order to study the contents of overpotentials of the oxygen electrode reaction at 865°C and 1050°C respectively. Two type of cell were constructed. One is the cell for measuring the Na_2O concentration overpotential, another is the cell for measuring the oxygen concentration over-potential both on the electrode interface. The results showed that the concentration over-potential from oxygen pressure difference amount to the total over potential by more than 95 %. This means the transport of oxygen in a melt controls the electrode processes. The behavior can be understood as the result of the existence of the oxygen electrode reaction.

I-3-2 Emf Measurements for Binary Oxide Mixtures

Emf measurements for binary oxide melts have been carried out by means of concentration cell of the following type with the help of the oxygen electrode reaction in order to study the behavior of the net-work modification in acidic oxide-rich composition.

$$(Pt)O_2 \mid A_2O \text{ in Acidic oxide (1)} \parallel A_2O \text{ in Acidic oxide (2)} \mid O_2(Pt)$$

where A_2O denotes an alkali oxide, the transports number of alkali ion are known unity in bulk. The following systems are studied and composition ranges are confined to a part of total composition by temperature, volatility and contamination (when alumina crucibles were used).

systems	mole fraction of A_2O	Temperature (°C)
Na_2O-P_2O_5	0.30 ~ 0.60	800
Li_2O-B_2O_3	0.03 ~ 0.40	925
Na_2O-B_2O_3	0.03 ~ 0.33	864
K_2O-B_2O_3	0.03 ~ 0.30	902

I-3-3 Abstract of Results and Discussion

The results of emf measurements of alkali borate are significant with respect to two points[38]. The first is the decrease of relative partial molar quantities, $\Delta\bar{H}^{excess}_{A_2O}$ and $\Delta\bar{S}^{excess}_{A_2O}$ for concentration from 100 to 85 mol % B_2O_3, which means the endothermic heat of B_2O_3 and positive partial excess enthalpies of B_2O_3. The second is the drastic increment of $\Delta\bar{H}_{A_2O}$ and $\Delta\bar{S}_{A_2O}$ 50 ~ 70 kcal and 30 ~ 40 e.u. respectively for concentrations 85 to 70 mol % B_2O_3.

Up to now thermodynamic explanations of activity of binary oxide mixtures are all carried out by using an unvariable equilibrium constant over all composition range for the reaction of net-work modification in spite of the concentrated solution as follows

$$\gtrless Si\text{-}O\text{-}Si \lesssim \; + \; O^{2-} \rightleftharpoons 2 \gtrless Si\text{-}O^{-}$$

$$K = \frac{[-O^{-}]^2}{[-O-][O^{2-}]} .$$

However the treatment can reproduce mostly the experimental data with respect to activities. From the present work, for the first time, it has been recognized that these partial molar quantities are not simple in campany with

calorimetric study by Kleppa et al. in such a high acidic oxide composition.

The present author proposed that the A_2O in borate or germanate and other net-work forming liquid, dissolved in associated state especially in high acidic oxide content about from 100 to 85 mol %. This model is supported by the following behaviors which are the low dielectric constant, long range interaction seeing from definite change of $\Delta\bar{H}^{excess}_{A_2O}$, $\Delta\bar{S}^{excess}_{A_2O}$ in dilute solution of A_2O, independent relation between the equivalent conductances and viscosities which can be seen in borates, the similarity with the conductances and its activation energies of associated ion in a oxide mixtures and the similar behaviors of $\Delta\bar{H}$ and $\Delta\bar{S}$ with the mixtures containing electric dipoles, which is n-heptane-ethanol solution. Thus the endothermic heat is considered from the coulomb interaction such as dipole-dipole interaction. The drastic increment of $\Delta\bar{H}_{A_2O}$ and $\Delta\bar{S}_{A_2O}$ for concentration from 85 to 70 mol % B_2O_3 are explained as collapse of four fold coordination and modification of net-works.

II DETERMINATION OF REVERSIBLE ELECTRODE REACTION FOR ELECTROMOTIVE FORCE MEASUREMENT

II-1 Preface

In the thermodynamic studies of the oxide melts such as borates, silicates, germanates, phosphates, the electromotive force technique has been applied on various occasions. However, difficulties in the construction of the reference electrode and especially the selection of the electrode materials, which specifies the well-defined electrode reaction, have retarded a wide use of this method, aside from the problem of the liquid junction potential.

Emf measurements in oxide mixtures show a very large variation in the potential with the composition of the melt. It is impossible in fact, to determine what is the reversible reaction by Nernst equation. Dietzel et al.[32] analysed their work in oxide melts according to the following electrode reaction

$$O^{2-} \rightleftharpoons \frac{1}{2} O_2 + 2e,$$

since they could measure successfully oxygen pressure when they constructed the following cell;

$$(Pt)O_2\ (P_{O_2} \neq 1\ atm) \mid Na_2O\text{-}B_2O_3 \mid O_2(Pt)\ (P_{O_2} = 1\ atm).$$

For the activity measurement

$$(Pt)O_2 \mid B_2O_3 \parallel \text{Borate} \mid O_2(Pt).$$

Flood, Førland and Motzfeldt criticized[34] the consideration of Dietzel et al. for their ambiguity what kind of reaction is potential determining. The present author considers the problem is what is the chemical species of reduced oxygen which can determine the electrode potential together with neutral oxygen in a melt.

Meanwhile, CaO-stabilized ZrO_2 has been proved to be an excellent solid electrolyte[35], which can be used to measure oxygen pressure in gaseous atmosphere[39], oxygen content in liquid metals[40] and so on. In the present study the ZrO_2(CaO) was used differently. The ZrO_2(CaO) was coupled with Pt-electrode, and the electrode reaction was forced to be the one as above mentioned.

II-2 Experimental

The measurement of the thermodynamic activity of Na_2O in Na_2O-B_2O_3 melt has been carried out with the following cell,

$$(Pt)O_2 \mid ZrO_2(CaO) \mid Na_2O\text{-}B_2O_3(I) \parallel Na_2O\text{-}B_2O_3(II) \mid ZrO_2(CaO) \mid O_2(Pt)$$

and its construction is shown in Figure 1 . The electrode reaction is given by

$$O^{2-} \rightleftharpoons \frac{1}{2} O_2 + 2e$$

because the $ZrO_2(CaO)$ is used as electrode constituent to carry O^{2-} ion exclusively. The potential gap across the interface between $ZrO_2(CaO)$ and melt is considered to be set up so as to equalize the electrochemical potential of O^{2-} in both phases. Further, as the transport number of Na^+ is known unity[41] through the liquid junction, the liquid junction potential is given by

$$U_{ljp} = -\left(\frac{1}{F}\right)\left(\mu_{Na^+(I)} - \mu_{Na^+(II)}\right)$$

where μ_{Na^+} is the chemical part of the electrochemical potential of Na^+ in the melt. Accordingly, the net electromotive force is represented as

$$E = \frac{1}{2F}\left(\mu_{O^{2-}(I)} - \mu_{O^{2-}(II)}\right) + \frac{1}{F}\left(\mu_{Na^+(I)} - \mu_{Na^+(II)}\right)$$
$$= \frac{RT}{2F} \ln \frac{a_{Na_2O(I)}}{a_{Na_2O(II)}}$$

where a_{Na_2O} is the thermodynamic activity of Na_2O. In Figure 1, platinum wire (A) is in electric contact with inside bottom of the zirconia tube, the latter being grooved for suspension. The corundum tube (C) which separates the two melts is furnished with a hole of 0.3 mm diameter at the bottom which constitutes liquid junction. The assembly in a reaction tube was heated in a resistance furnace in air atmosphere. A stainless tube was introduced between the furnace tube and the alumina reaction tube and was grounded. The voltage was measured both by an ordinary potentiometer YOKOGAWA 2722 type and by a vibrational reed electrometer (TAKEDA RIKEN TR-84M type). It took about 4 hr for the emf to approach close to constant value. Usually the measurement was carried out in 12 hr after the charge. It remained constant for several days. The sample melt was prepared from H_3BO_3 and Na_2CO_3 of the guaranteed reagent grade. The solubility of CO_2 is too small according to Pearce's data[42]. Though H_2O are known to be slightly soluble according to Franz [18], the contribution to the total conductivity were checked to be negligible by means of conductivity measurement. The type of cell for conductivity measurements are shown in Figure 2. The samples were prepared from H_3BO_3 and Na_2CO_3 just like the emf measurement. The data obtained are given in Figure 3. The electric conductance, which might permit the conductance of H^+,

was consistent with what the water were removed at sufficiently higher temperature[5]. *This means the contribution of H^+ is negligible over the experimental range of composition. Temperature were measured by Alumel-chromel thermocouple which had been calibrated against the melting points of Sn, Pb, Al, and NaCl. The compositions of the melts were determined by flame photometry within ±0.25 mol % for Na_2O.

(* see page 64)

II-3 Results and Discussion

The measurement was carried out for the Na_2O-B_2O_3 melt over the composition range 0.65-0.95 by mole fraction of B_2O_3, the melt of 0.95 being used as a reference. The results are shown in Figure 4 . The data obtained from the measurement with the bare platinum wire without the zirconia tube are also plotted. Only small deviation is found in the two sets. Stegmaier and Dietzel[33] have measured the activities of Na_2O, in sodium borates with a cell in which platinum wire electrodes were dipped into the melt. The data are reproduced in Figure 4 , where the emf value is shifted for easier comparison, although they measured it referred to 0.5-0.7 m/o alkali oxides. The order of magnitude and tendencies of emf values are in fair agreement among the three sets of data.

It has been known that oxygen ion in a melt takes part in Pt-electrode reaction at equilibrium but has not been known what is the ionic constituent of oxygen ion. The present consistency between Pt-electrode with $ZrO_2(CaO)$ and Pt-electrode show it is oxygen ion, O^{2-}, in Pt-electrode. This consistency suggests two facts. First, either the oxygen pressure in the melt at the platinum electrode without the ZrO_2 tube is in equilibrium with gaseous atmosphere or the electrode potential is determined practically at the gas-metal-oxide coexisting surface on the platinum wire. Second, the assumption that the electrochemical potential of O^{2-} is at the same level across the ZrO_2-melt interface is correct. In passing, one must note that the magnitude of emf corresponds to 10^7 of the activity ratio at 0.65 to 0.95 m/o B_2O_3. This drastic change reminds one of the hydrogen ion concentration in an aqueous solution. This behavior is not observed in typical binary melts and will be understood better in terms of the acid-base character of the melt. Thus, while O^{2-} from Na_2O neutralizes B_2O_3 to various degrees depending upon the strengths of basicity and acidity of Na_2O and B_2O_3 respectively and upon their compositions.

The features of this electrode are the following. (i) The oxygen pressure is well defined. Although platinum or graphite rod electrodes have been used in the investigations of this kind, the pressure of O_2 or

CO has not been specified except in a few cases[43].
(ii) Since there is no electronic conduction through the ZrO_2 phase, the oxygen dissolved in the melt cannot take part in the electrode reaction. This gives an advantage that the fugacity of molecular oxygen in the melt can be handled freely, being independent of the basic oxide content. A procedure of this sort becomes important, when one wishes to measure the concentration ratio of Fe^{2+}/Fe^{3+} as functions of oxygen pressure and the basicity of an iron-containing melt separately. Parenthetically, the fugacity of molecular oxygen in the melt can be measured by the ordinary technique with ZrO_2[44].
(iii) The possible contamination due to ZrO_2-melt reaction is a shortcoming, as this might give rise to interference in reversibility of the emf with respect to O^{2-}. In the present system zirconia showed a much higher resistance against contamination than sintered corundum.

The present method will widen the applicability of the emf technique to systems for which otherwise reversible electrode cannot be constructed. This electrode will function well as the reference electrode when one might want to measure a single electrode potential of a cathode in electrolysis of an oxide melt. There is no need of bubbling of O_2 gas on the surface of the electrode[45]. This electrode is in principle analogous to the glass electrode in a pH meter in which a thin glass layer functions reversibly only to hydrogen ion.

Figure 1. Cell for Na_2O Activity Measurement

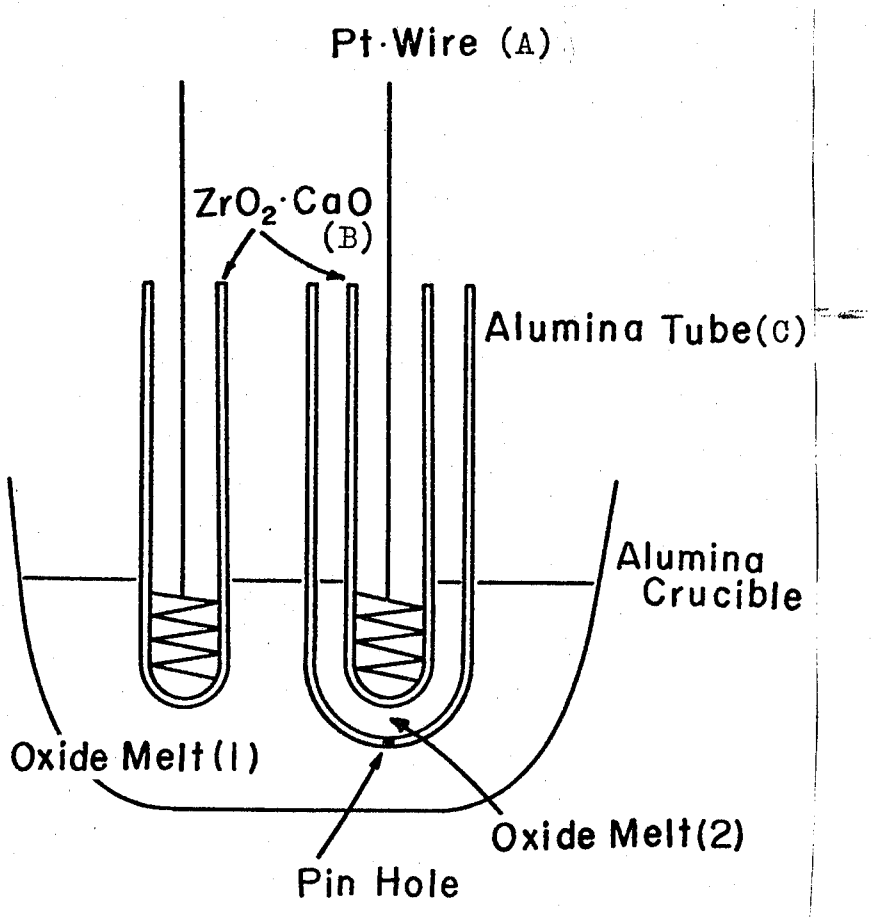

Figure 2. Cell assembly for conductivity measurement

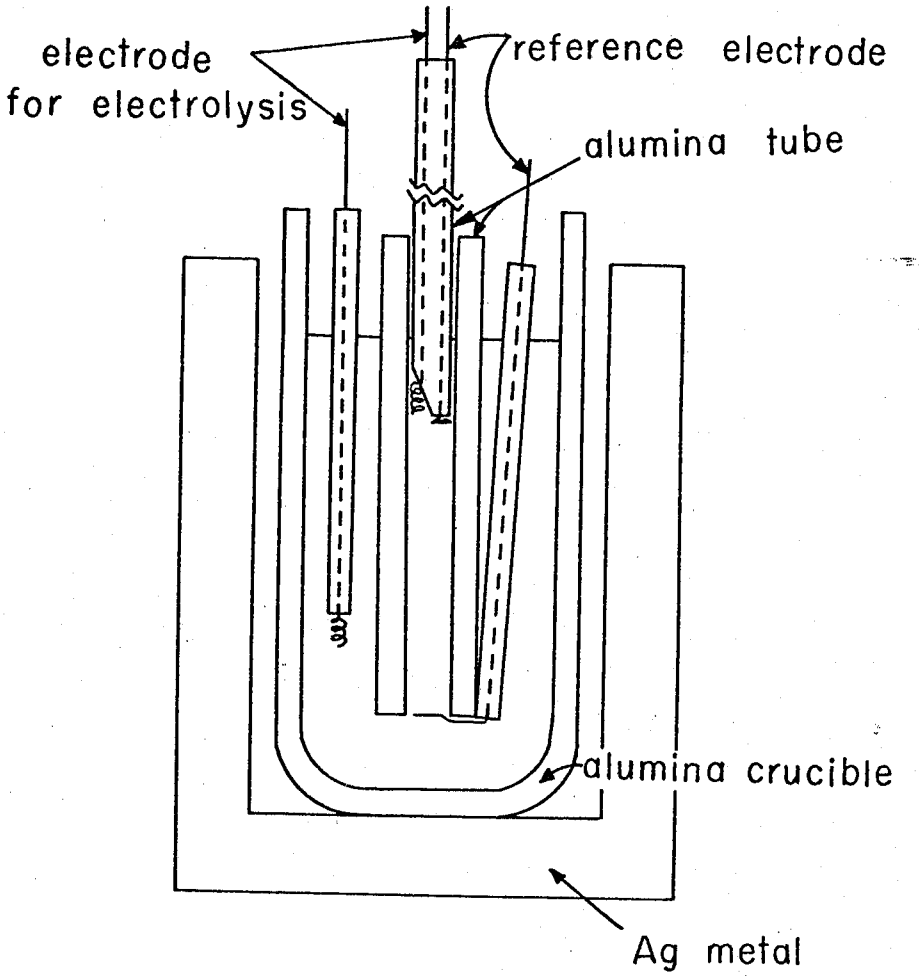

Figure 3. Electrical conductivity of Na_2O-B_2O_3 melts at 900 °C

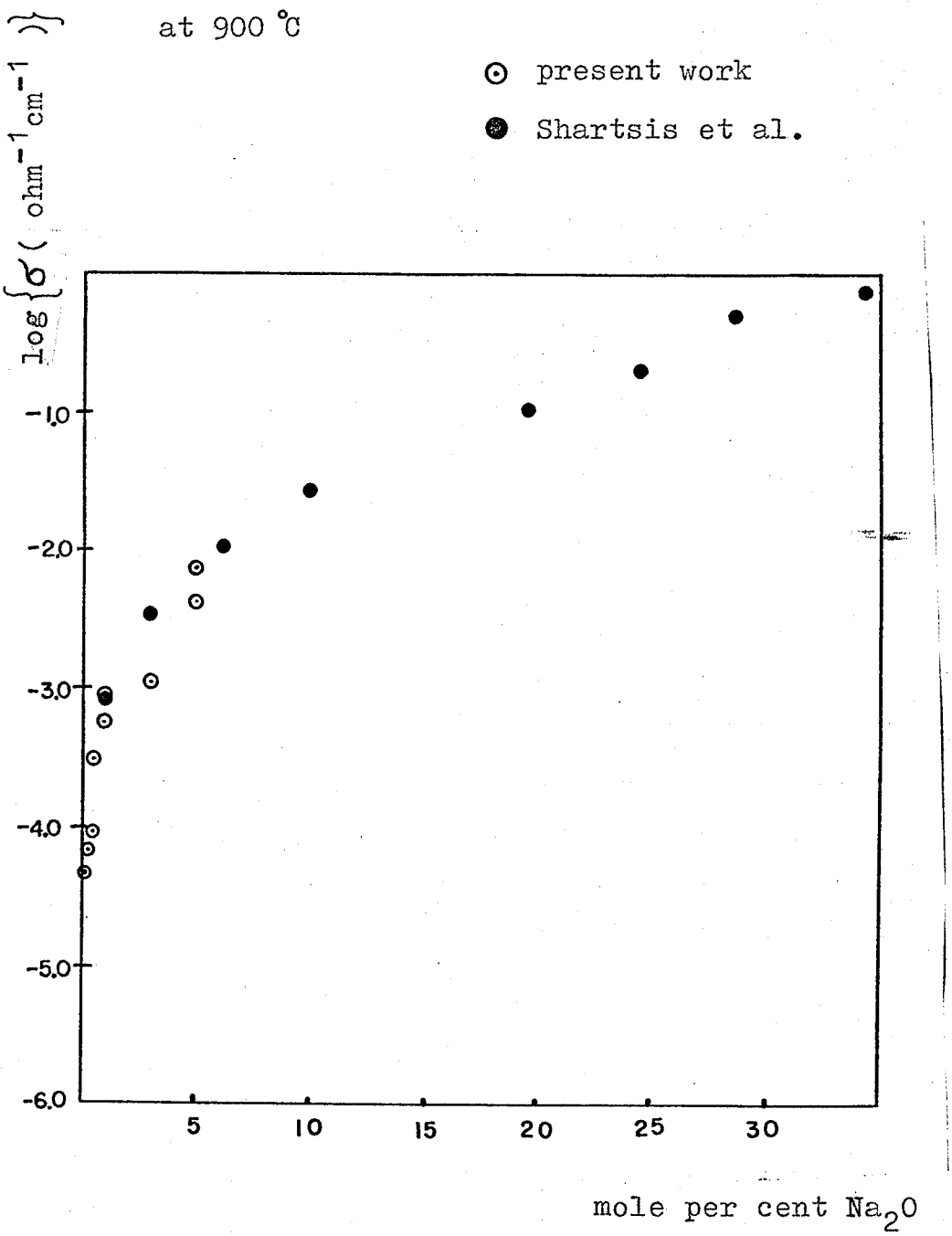

Figure 4. Emf value as functions of composition at 850° C

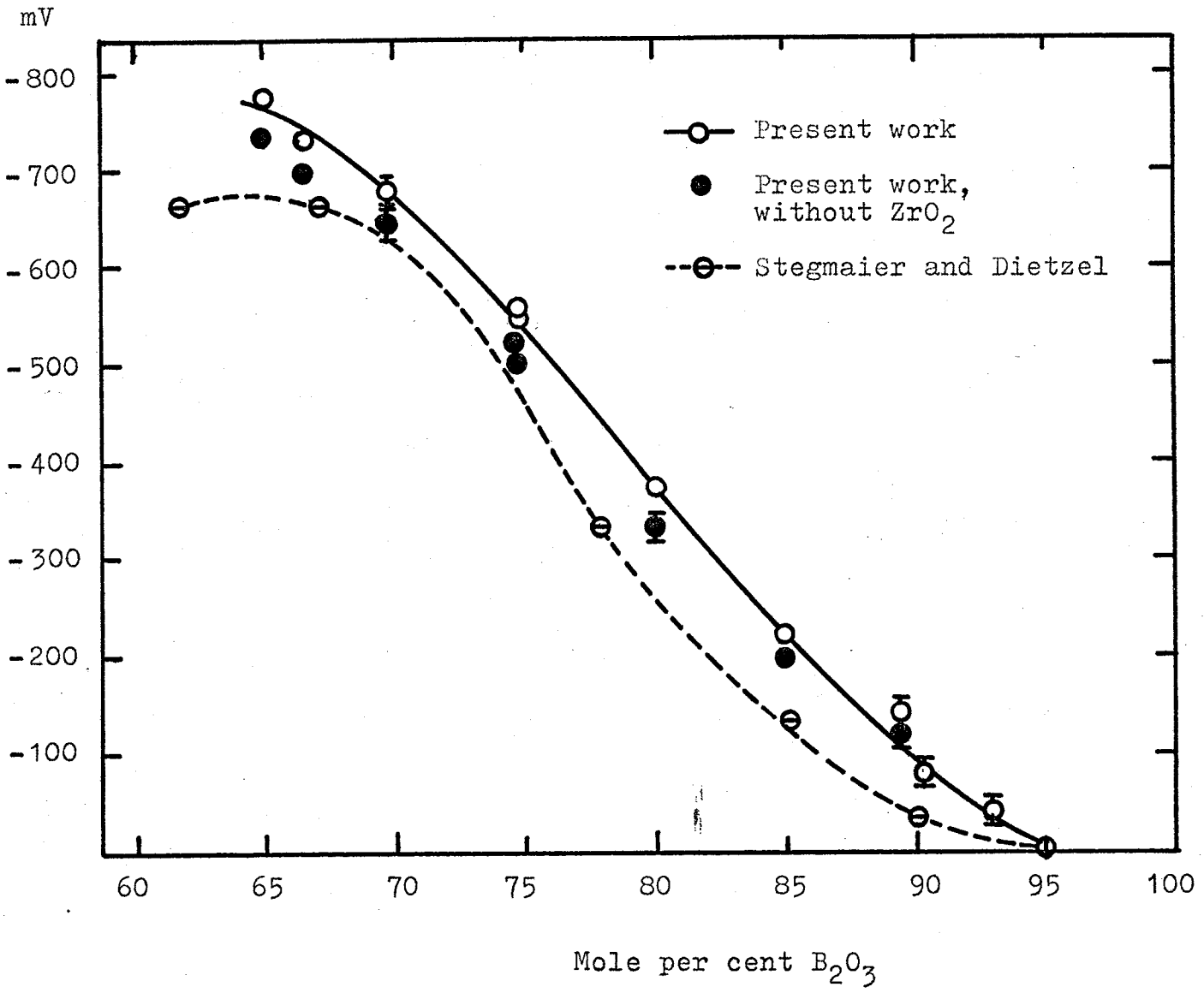

III ELECTRODE KINETICS IN BINARY OXIDE MELTS

III-1 The Measurement of Na_2O-concentration Overpotential

III-1-1 Preface

Slag-metal reactions at high temperature can be conveniently treated as an electrode process, as has been exemplified by the work by King and Ramachandran[10].

If we restrict our attention to liquid oxide-metal systems, one of the most basic reactions is the oxygen electrode reaction, especially if the metal electrode is noble.

$$O^{2-} \rightleftharpoons \frac{1}{2} O_2 + 2e$$

Dietzel and his co-workers[32,33] analysed their work in alkaline oxide-boric oxide mixtures according to this reaction, Later Førland et al. criticized their treatment[34]. However as is shown in the previous chapter this reaction has been shown to determine the potential[36].

Any electric current through the electrode at a nonequilibrium state usually gives rise to overpotentials of various sorts. These are also quite important from the viewpoint of such subjects as interfacial phenomena at reacting slag-metal interfaces.

In this chapter a novel device is reported which differentiates the overpotential due to the Na_2O concentration gradient from the others (due to oxygen pressure gradients or the activation overpotential, etc.). In the field of oxide-metal systems, Gosh and King[43] and Kawakami and Goto[44] have studied the electrodic behavior of Pt in silicate melts and indicated the transport of oxygen in the silicate to control the rate of the process.

III-1-2 Experimental Methods

As is stated in the foregoing section, any net current through an electrode gives rise to various overpotentials. Thus it is the main problem to determine which overpotential is decisive in the process under study. Although various methods including transient methods have been applied to this type of problem, the results have not always been satisfactory.

In the present method, a subsidary electrode (melt | ZrO_2(CaO) | O_2(Pt)) picks up the chemical potential of alkaline oxide not through a diffusion layer, if any, but just at the working electrode surface. A similar method has been applied to an aqueous hydrogen electrode system, and the high permeability of the hydrogen through

the electrode metals was used with advantage.

The principle is shown schematically in Figure 5. Around the working electrode (W.E.), a concentration gradient will be presumably set up at a steady state, as well as an activation overpotential, etc. The reaction products at the electrode stagnate on one side which is enveloped with the W.E. net and the stabilized zirconia wall, and an ordinary diffusion layer will be built up on the other side. As the reference electrode (R.E.(2)) is independent of the melt, the reference electrode (R.E.(1)) coupled with R.E.(2) provides a cell

$$O_2(Pt) \mid ZrO_2(CaO) \mid \text{melt (bulk)} \parallel$$

$$\text{melt (at W.E.)} \mid ZrO_2(CaO) \mid O_2(Pt)$$

whose emf is given by

$$\Delta E = -\frac{RT}{2F} \Delta\mu_{Na_2O}$$

as only Na^+ is the charge carrier in the oxide melt. The emf between W.E. and R.E.(2) does not in general give the oxygen pressure at the W.E. surface since the activation overpotential might have to be added.

III-1-3 Experimental

In Figure 6 and 7 are shown the cell assembly and the emf measuring as well as the electrolyzing circuits. The working electrode (W.E.) is a platinum wire (0.3 mm in diameter and 120 cm in length) which is wound tightly and compactly around a stabilized zirconia tube. The latter (with a platinum wire inside) functions as a reference electrode (R.E.(2)). Another reference electrode (R.E.(1)) was used in the form of a bare wire since this electrode fulfills the condition that it should be reversible with respect to the O_2/O^{2-} reaction just like the (melt $|ZrO_2(CaO)|O_2(Pt)$) oxygen electrode and it is much easier in the construction of the cell compared with a zirconia tube.

The cell assembly was heated in a resistance furnace. The temperature was kept at 865 ± 3°C. A grounded stainless steel tube was introduced between the furnace tube and the quartz reaction tube containing the cell. The sodium borate oxide electrolyte was prepared from boric acid and sodium carbonate both of guaranteed reagent grade. Powder mixtures of the desired composition were heated at about 900°C in a platinum crucible to remove water and carbon dioxide. The liquid oxide was then poured on a stainless steel plate and the glassy material was crushed before use.

In this study only steady state measurements were performed. It took 1 to 2 hr for the current to become constant at anodic polarization, while 2 to 3 hr was needed at cathodic polarization.

This method is based on the assumption that the electrochemical potential of O^{2-} at the working electrode surface is uniform throughout the stagnant melt between the Pt coil and the zirconia wall. In the present viscous melt, the Nernst diffusion layer will be much thicker than in a usual aqueous solution (10^{-3} cm at a stirred condition)[46]. On the other hand, the zirconia tube is tightly and compactly wound with the electrode wire. The distance between the neighbouring wires of the electrode coil must be shorter than the diffusion layer thickness. The diffusion length from the electrode surface to the zirconia wall is finite. Therefore, the activity of Na_2O in the open space between the wall and the electrode coil becomes equal to that at the electrode coil surface after a sufficient time, while on the outer side of the coil the normal diffusion layer is set up. Furthermore, the electrode coil permits the ionic Na^+ current to migrate through the coil's gap. That is the reason why not a foil but a coil was used as the electrode in this experiment. Thus the above device can pick up the overpotential due to an Na_2O activity at the working electrode surface.

III-1-4 Results and Discussion

The typical data on the measurements are listed in Table 1. The emf values between the reference electrodes R.E.(1) and R.E.(2) correspond to the concentration overpotential of Na_2O. The data in Table 1 have been corrected for zero current voltage due to the dissimilarity of the two electrodes, (R.E.(1) is 5 ~15 mV positive against R.E.(2)). It should be noted that the emf is quite small as compared with the total voltage. This is especially true for the cathodic polarization experiment. The iR drop was determined to be very small as measured by the galvanoststic method[43]. The resistance of the cell with 5 mol % Na_2O melt was 22 ± 2 and decreases with Na_2O content. So the iR drop was neglected except in the cases of anodic polarization at 5 mol % Na_2O melt. The corrected values are shown in parentheses in Table 1.

So far the current density has not been considered, since difficulties were encountered in estimating the contribution of the gas-melt-electrode three-phase boundary to the total current. The melt creeps up along the electrode wire and the current at the gas-melt boundary is exceedingly large, especially in the cathodic polarization experiment. In Figure 8 is plotted the current-voltage relation for a cell, in which a platinum

wire of 1 mm diameter was just in contact with melt surface on the one hand, and the same relation for a second cell in which the wire was dipped 1 cm into the melt. The fact that the two sets of data lie close together at the cathodic polarization suggests that the contribution from the W.E.-interface is considerable. However, as is shown in Figure 6 , the cell assembly was set up in such a way that only the dipped part of the working electrode is in contact with the zirconia tube and the reference electrode (2) picks up the inner melt-electrode reaction only. The current from the reactions at the melt-gas-electrode interface under study independently or in parallel at the applied voltage, since any discharge process like convection and/or diffusion in vertical direction can be neglected. However, if such mixing would occur, it would strengthen apparently the overpotential of Na_2O. Therefore, there is no ambiguity in the above discussion of the overpotential.

The conclusion is that the overpotential must have an origin other than the concentration gradient of Na_2O. The present authors feel that the overpotential comes from the concentration gradient of oxygen, since the emf between the working electrode and the reference electrode (2) amounts to almost the total overpotential and at the high temperatures an activation overpotential does not seem to be established at steady state conditions. In this

way, the present study substantiate the oxygen electrode reaction from the view point of electrolysis. The oxygen pressure at the electrode is calculated to be 10^{-10} atm., if the overpotential of, say, 565 mV is assumed to arise solely from the oxygen pressure gradient in the cathodic polarization experiment at this temperature. However, the molecular state, of the oxygen responsible for the overpotential i.e. O_2, O_2^-, O_2^{2-}, is not clear at present.

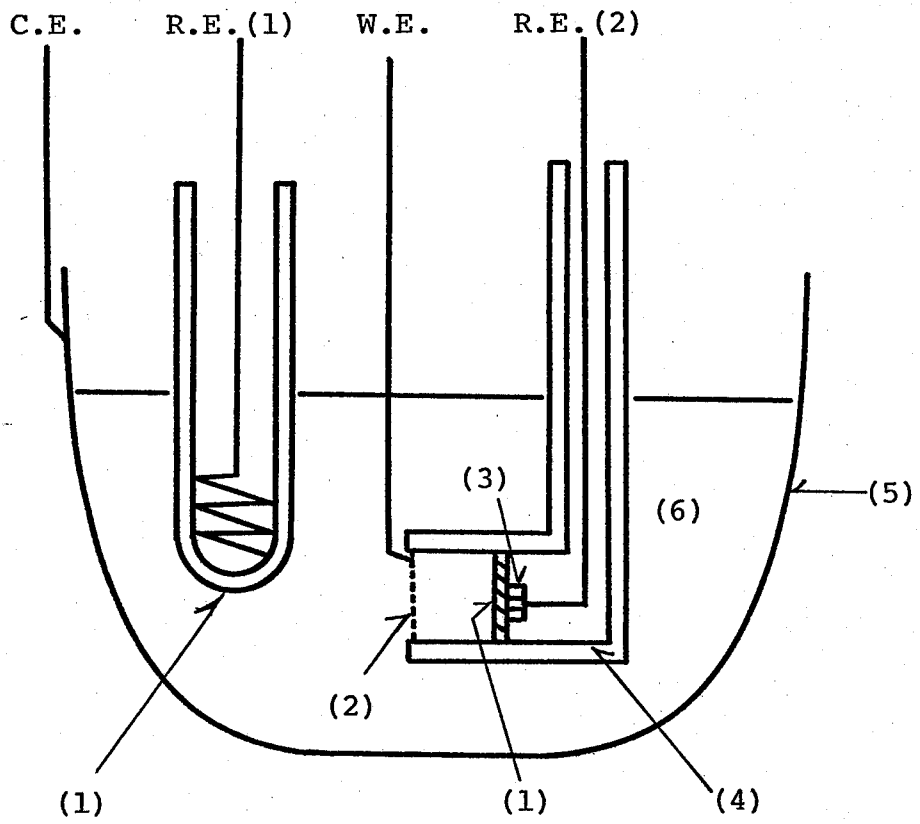

Figure 5. Cell construction to show measuring principle of Na_2O concentration overpotential

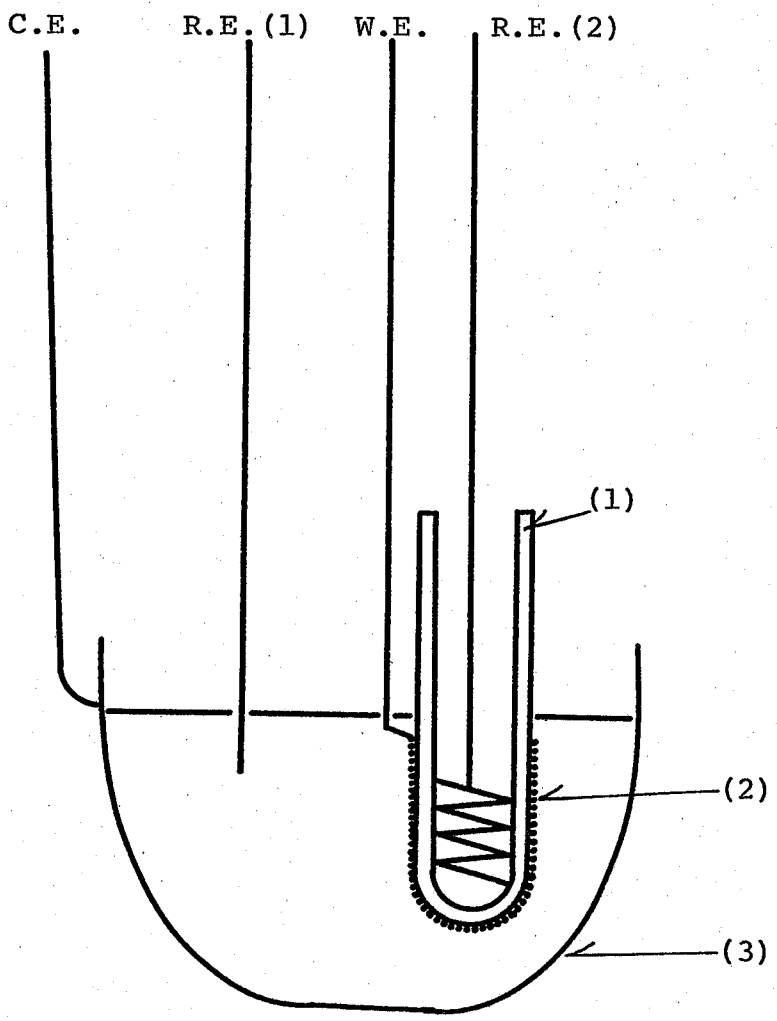

Figure 6. The actual cell assembly for measurements of Na_2O concentration overpotential

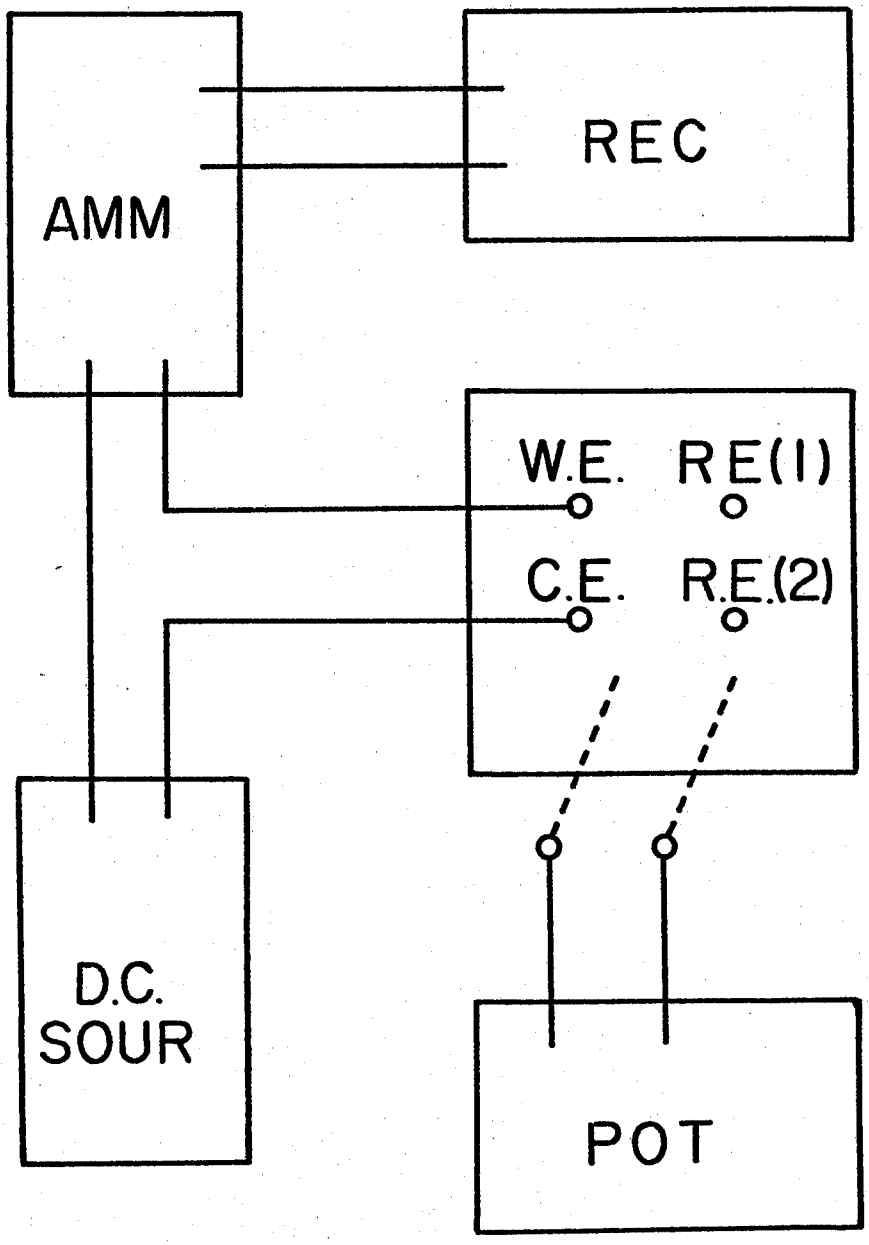

Figure 7. Schematic representation of the electrical circuit including of the cell.

REC : Recorder AMM : Ammeter

D.C. SOUR : D.C. power source

POT : Potentiometer

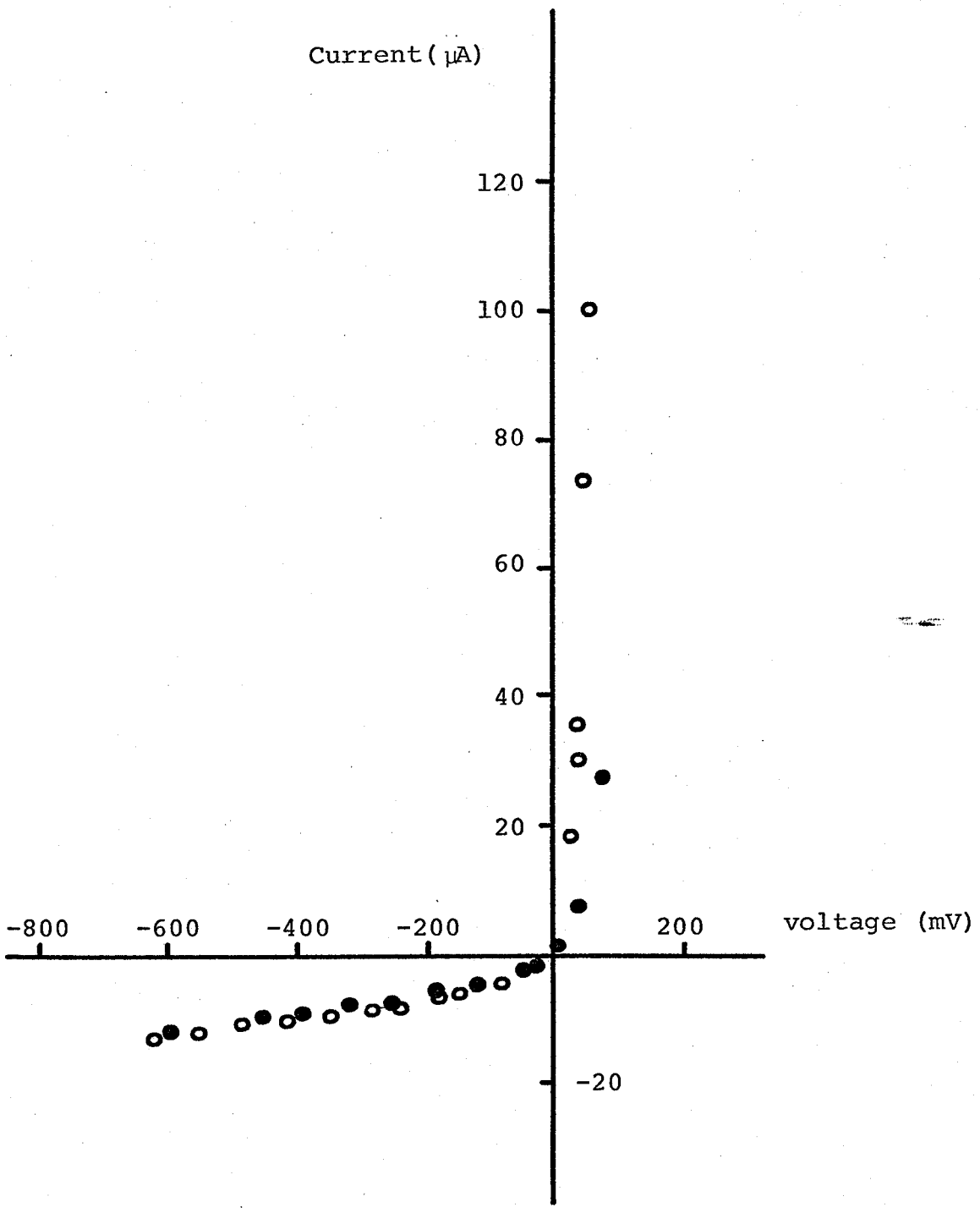

Figure 8. Current-voltage curves at 5 mol % Na_2O-i5 mol % B_2O_3 865±3°C.

o Pt electrode, 1 cm dipped

• Pt electrode, just in contact on surface of the melt

Table 1. Electromotive force measurements (emf between R.E.(1) and R.E.(2)) corresponding to Na_2O concentration overpotential in total overpotential

Cathodic Polarization				Anodic Polarization			
Current (μA)	emf between W.E.&R.E.(1)	emf between W.E.&R.E.(2)	emf between R.E.(1)&R.E.(2) R.E.(1):positive	Current (μA)	emf between W.E.&R.E.(1)	emf between W.E.&R.E.(2)	emf between R.E.(1)&R.E.(2) R.E.(1):positive
(1) 5 Mol % Na_2O, 95 Mol % B_2O_3							
-10.3	-103	-101	+2	+190	+50	+43	-4(-2)
-16.0	-304	-298	+5	+370	+62	+48	-12(-2)
-21	-502	-496	+5				
-31	-700	-692	+10				
(2) 10 Mol % Na_2O, 90 Mol % B_2O_3							
- 5.5	-137	-136	0	+ 38	+38	+40	0
-10.5	-337	-333	+2	+155	+54	+54	-2
-16.2	-731	-725	+7				
-12	-608	-585	+8				
- 1.2	-197	-192	+7				

(continued)

(3) 15 Mol % Na_2O, 85 Mol % B_2O_3							
- 3.0	-176	-177	+1	+ 98.7	+52	+47	-4
- 4.4	-259	-257	+2				
- 7.8	-406	-405	+5				
(4) 25 Mol % Na_2O, 75 Mol % B_2O_3							
- 4.7	-160	-152	+8	+115	+56	+55	-1
- 9.2	-347	-346	+3	+242	+72	+69	-5
-14	-539	-535	+5				
(5) 33 Mol % Na_2O, 67 Mol % B_2O_3							
- 3.7	-119	-116	+6				
-10	-206	-200	+3	+ 52	+37	+45	+8
-75	-355	-350	+1	+205	+46	+52	+5
-280	-443	-436	+6				

Values in ( ) have been corrected for iR drop.

III-2 The Measurement of Oxygen Overpotential

III-2-1 Preface

In order to clarify the behavior of the oxygen electrode reaction, the another electrolysis experiment has been carried out at the stationary state for measurements of the oxygen pressure difference between an electrode interface and the bulk of the oxide melt.

Silicon, phosphorus, carbon, sulfur etc. dissolved in liquid metal can move through interface between liquid metal and liquid oxide. This reaction usually depends on oxygen pressure and basicity of the oxide melt. As the matter of fact, the basic slag is used exclusively for steelmaking in order to eliminate phosphorus, sulfur etc. Thus, the time dependence of oxygen pressure at the interface, which arises from electrolysis or from other thermodynamic potential differences, is very important for the reaction and mass transport including electrode system.

Recently, King et al.[43] carried out anodic electrolysis in a Li_2O-SiO_2 melt in stationary state of current and indicated the diffusion of oxygen, dissolved in the melt, controls the electrodic process in comparatively low current. By means of rotating electrode or by transient method similar results have been reported apart

from the quantitative data of the overpotential. The present author has avoided the experiment with the large current at the gas-melt-electrode coexisting part, which makes it difficult to determine current density, and deviced an appropriate electrode system to measure quantitatively the oxygen pressure gradient at electrode interface.

III-2-2 Experimental

It is well known that atomic oxygen is readily soluble in liquid Ag[47], Cu[48], Fe[49], Pb[50], Sn[51] etc. Silver was selected as electrode, because it is comparatively noble and because considerable amount of oxygen is soluble. It was tried to dissolve oxygen in liquid Au but the measurement was unsuccessful.

The cell which is shown in Figure 9 were constructed. Prior to electrolysis the following reaction is in equilibrium,

$$Ag + O_2(\text{in oxide melt}) = Ag_2O(\text{in oxide melt}).$$

In other word,

$$P_{O_2}(\text{in oxide melt}) = P_{O_2}(\text{in liquid Ag}).$$

When cathodic polarization is carried out, the reaction proceeds to the following direction.

$$\frac{1}{2}\,O_2(\text{in oxide melt}) + 2e(Ag) \longrightarrow O^{2-}(\text{in oxide melt})$$

The decrease of oxygen pressure is considered to appear at the interface of the electrode and dissipate gradually into the bulk phases of both liquid Ag and oxide melt, in such a way as illustrated in Figure 10. Since the diffusion of oxygen in liquid silver electrode is semi-infinite type as shown in Figure 9, after the sufficient time the oxygen pressure in liquid silver will reach a uniform value which is the same as the pressure at the silver-oxide melt interface. The oxygen pressure versus that of the bulk oxide melt is the concentration over-potential of Ag oxygen electrode reaction. Anodic polarization is considered similarly. The principle of the measurements of the oxygen pressure in liquid Ag electrode is as follows

$$(Pt)O_2\ (air) \mid ZrO_2(CaO) \mid \underline{O}(Ag)$$

$$E = -\frac{RT}{4F} \ln \frac{a_O^2(Ag)}{P_{O_2}(air)}$$

Na_2O-B_2O_3 melts were selected as sample melts at

first. Alumina crucible was attacked severely in all range of the possible Na_2O-B_2O_3 composition. Especially in B_2O_3 rich composition, the erosion was much more severe and holes were digged in a sintered alumina crucible within half a day at about 900°C. Later, Na_2O-B_2O_3 was replaced by Na_2O-$2SiO_2$. The crucible for this system was kept in safe more than three days at about 1100°C.

In order to ascertain whether oxygen pressure in liquid Ag with $ZrO_2(CaO)$ can be measured exactly, the diffusion coefficient of oxygen were measured electrochemically and compared with some reported data. The assembly for the diffusion measurement is represented in Figure 11. At first the N_2 gas, which had been passed through heated Cu, Cu_2O to exclude oxygen, were derived over solid silver and then the cell was heated 1050°C. After the ratio C_o(in Ag)/C_o(1 atm) $\ll 10^{-3}$ had been confirmed by voltage measurement, the N_2 gas over liquid Ag were substituted by oxygen and the time dependence of the voltage were measured continuously with vibration reed electrometer and normal potentiometer.

The obtained data was analysed in accordance with the following equation,

$$E = -\frac{RT}{2F} \ln \frac{C_1}{C_o}$$

where C_o is the concentration of oxygen atom at the

surface of the liquid Ag under atmospheric oxygen pressure or air; C_1 is the oxygen atom concentration at the ZrO_2(CaO) surface. Since the reaction

$$O_2(\text{gas}) \rightleftharpoons 2O(\text{Ag})$$

is at equilibrium,

$$K = \frac{a_{oxy}^2}{P_{O_2}}, \qquad a_{oxy} = \sqrt{KP_{O_2}}$$

Further, since solubility of oxygen is considered to be sufficiently small,

$$C_{oxy} = \text{const}\sqrt{P_{O_2}}$$

In this experimental condition, oxygen concentration in the region $0 \leq X < L$ is initially zero, and the surface of liquid Ag($X=L$) are kept at a constant oxygen concentration which is in equilibrium with oxygen gas.

$$\frac{C_1}{C_o} \cong 1 - \frac{4}{\pi} \exp\left(-\frac{D\pi^2 t}{4L^2}\right)$$

holds[52] for time dependence of $\frac{C_1}{C_o}$ and leads to

$$D = -\frac{4L^2}{\pi^2 t}\left\{\log\frac{\pi}{4} + \log\left(1-\frac{C_1}{C_o}\right)\right\}$$

D is the diffusion constant of oxygen atom in liquid Ag; L is the depth of Ag. The obtained data of the diffusion constant of oxygen atom was 4.7×10^{-5} cm^2/sec at $1047 \pm 3°C$ the reported data is $0.46 \sim 3.3 \times 10^{-4}$ cm^2/sec[53] at 1050°C. Accordingly, electrode with $ZrO_2(CaO)$ was regarded to be appropriate to measure oxygen pressure in liquid Ag.

III-2-3 Results and Discussion

When a constant potential was added cathodically by potentiostat, as shown in Figure 13, the potential difference between reference electrode(2) and working electrode appeared gradually and approached to the added potential by potentiostat, like Figure 13. Until the oxygen potential become equal over all region of liquid Ag electrode, the potential is not well-defined. After more than 5 hours, the potential and current approached to a constant value, which is tabulated in Table 2 with the overpotential by potentiostat. Then the circuit were opened. The potential between the reference electrode(2) and working electrode does vary very slowly and it takes more than three days to recover the initial state. This shows the oxygen pressure in liquid Ag electrode have decreased actually, by cathodic polarization. The reference

electrode(1) was not always fine and the voltage of R.E.(1) is usually greater than R.E.(2) by 40 to 60 mV. In Table 2 , this uncertain potential is not corrected. The Pt-zirconia electrode or Ag electrode could function between as a reference electrode. However, on account of the very small space of the cell, the bare Pt oxygen electrode was used as a reference electrode. In Table 2 , the thermo-electromotive force is corrected where the potential of Stainless Steel wire as working electrode was 15 mV positive than Pt-lead wire.

In anodic polarization under large overpotential like Figure 14, an unstable curve of potential appeared which was considered as the result of oxygen bubble formation, while in the case of small anodic overpotential, clear differentiation of oxygen overpotential from the total overpotential could not be found, on account of the uncertain potential as mentioned above.

But from the Table 2 , especially in cathodic polarization at least 90 ~ 95 % of total overpotential is attributable to oxygen concentration overpotential at Ag electrode interface. Na_2O-$2SiO_2$ scarcely differ from sodium borate melts as a medium for oxygen diffusion. In addition to previous experiment in these oxide melts, the Pt-oxygen electrode reaction is the potential determining reaction and by the reaction, the oxygen overpotential arises. The following emf measurements

for study of the physico-chemical properties as a solution are analysed based on the Pt-oxygen electrode reaction.

Figure 9. Cell assembly for measurement of oxygen concentration overpotential

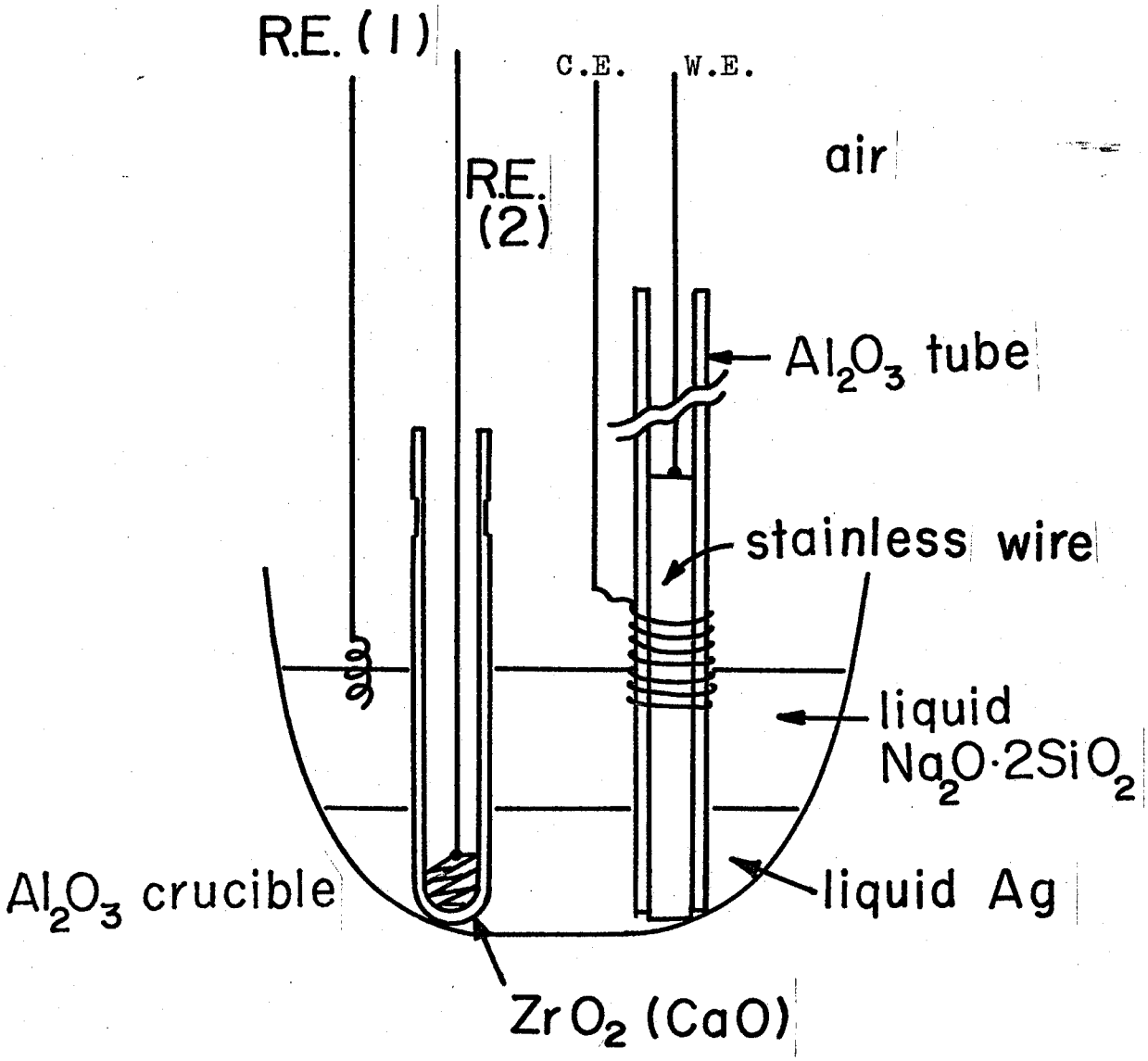

Figure 10. Schematic representation of oxygen transfer at Ag electrode

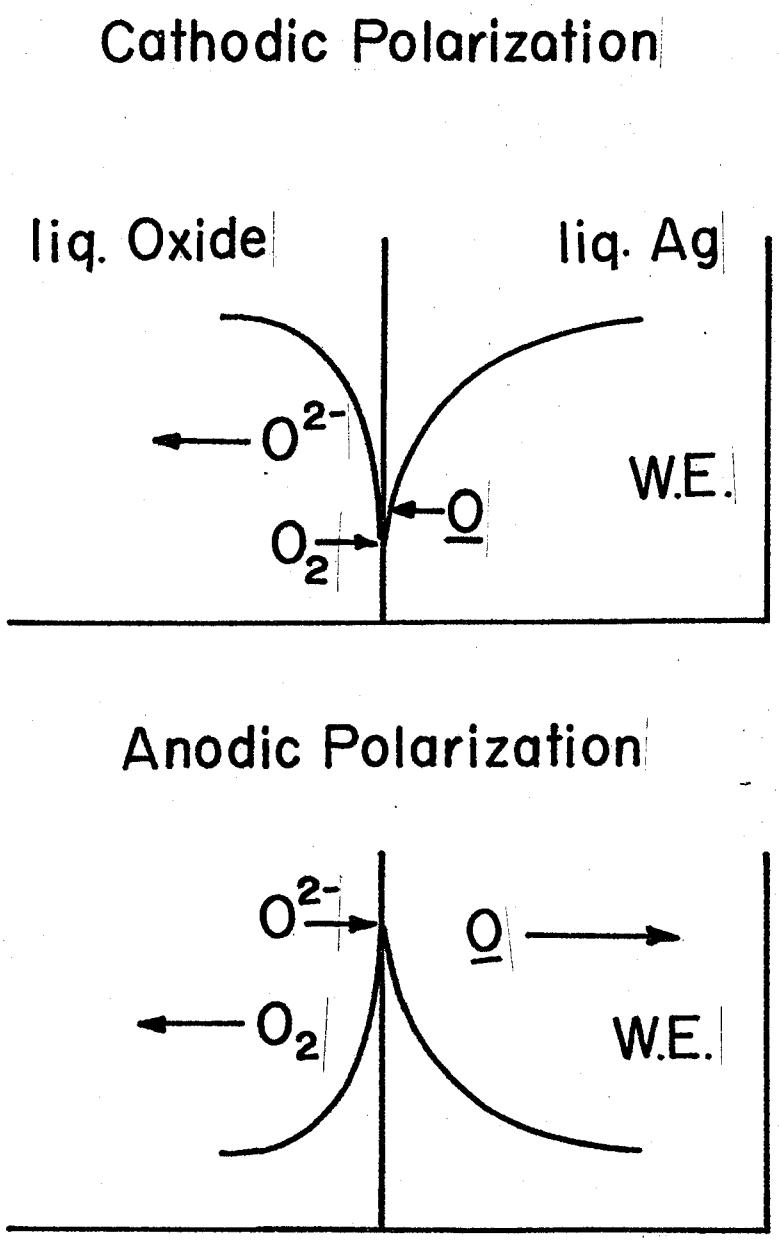

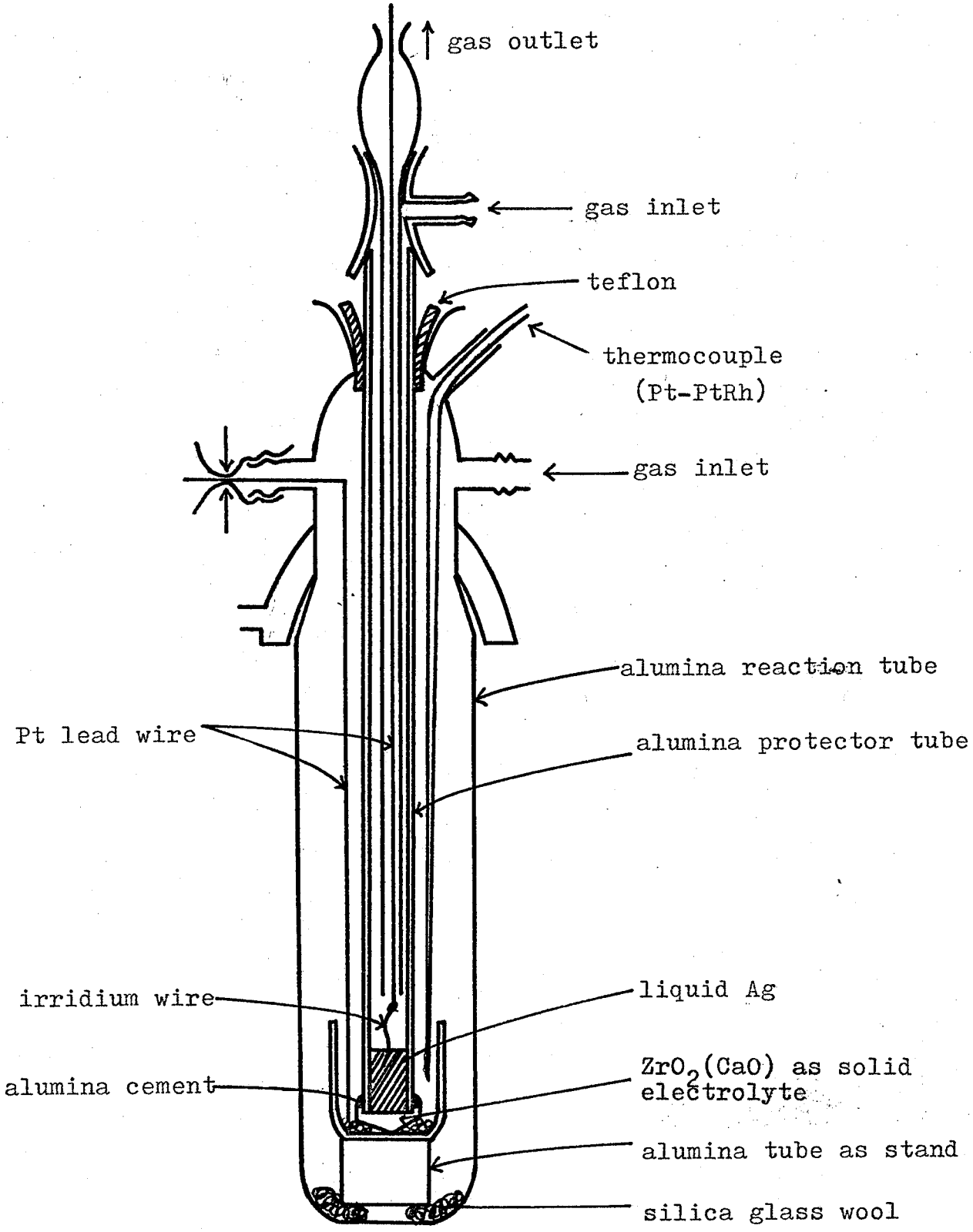

Figure 11. Cell assembly for measurement of diffusion of oxygen in liquid Ag

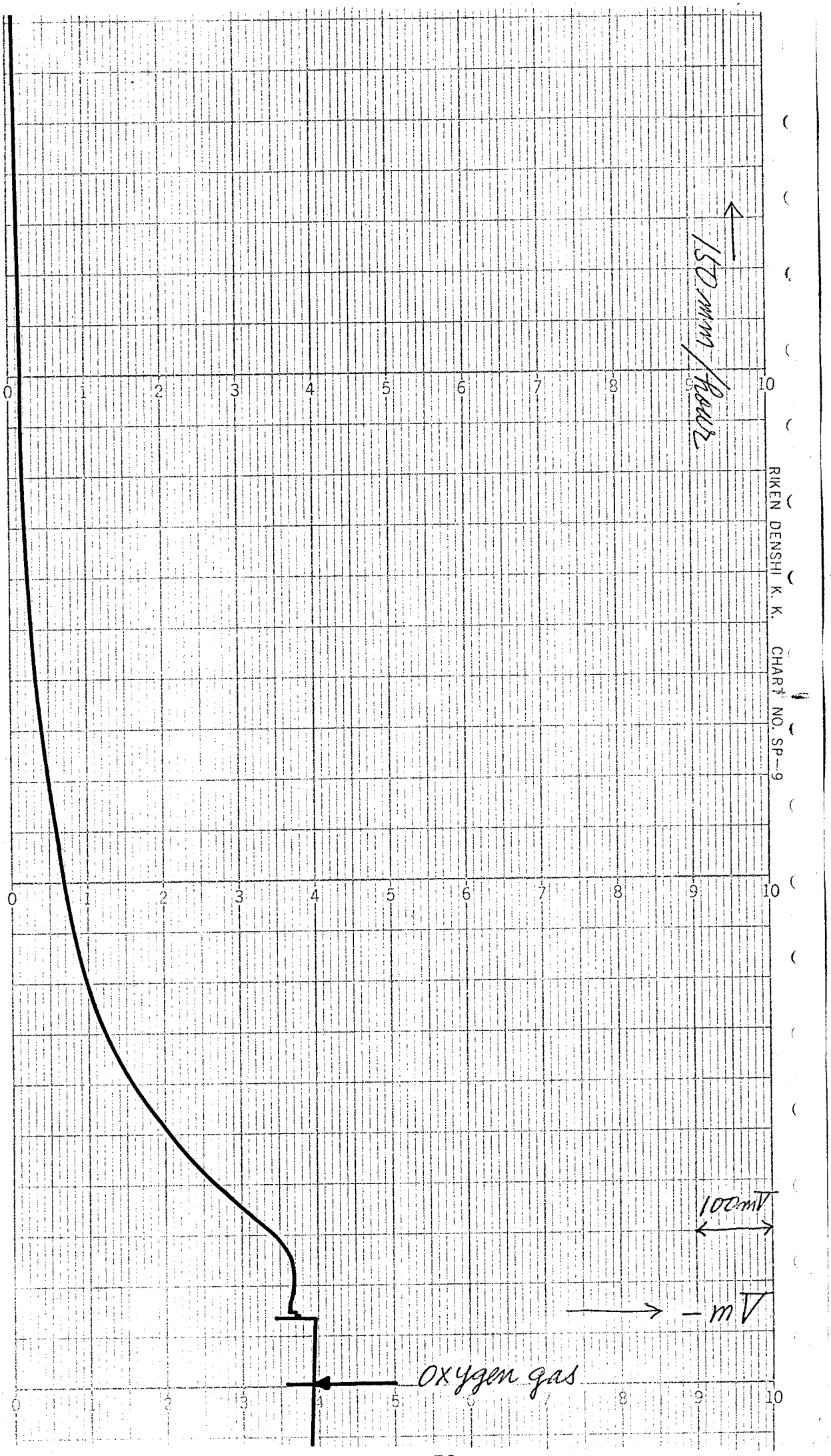
150mm/hour
RIKEN DENSHI K. K. CHART NO. SP-9
100mV
-mV
Oxygen gas

Figure 13. Time dependence of emf between working electrode and reference electrode(2) in cathodic polarization.

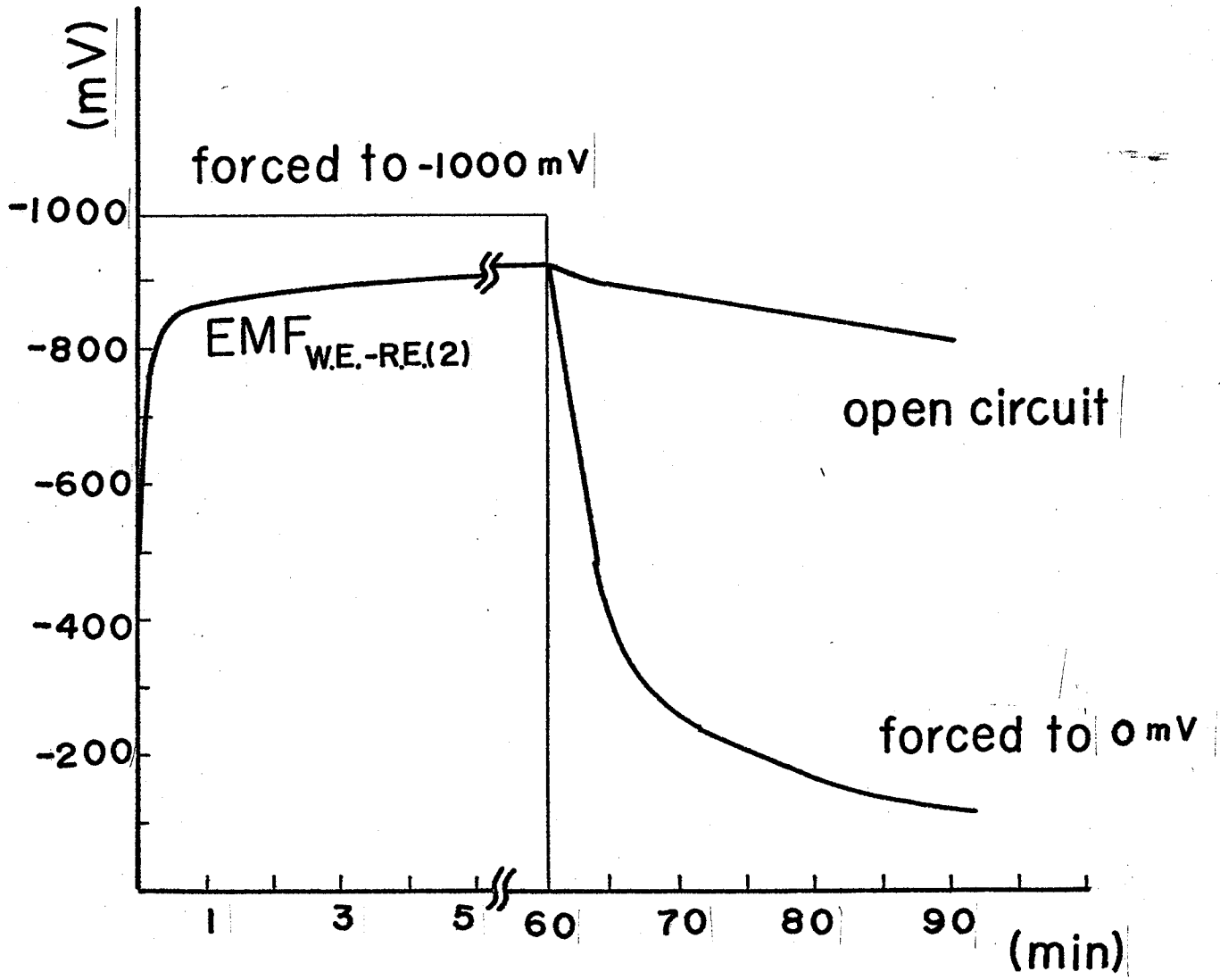

Figure 14. Time dependence of emf between working electrode and reference electrode(2) in anodic polarization

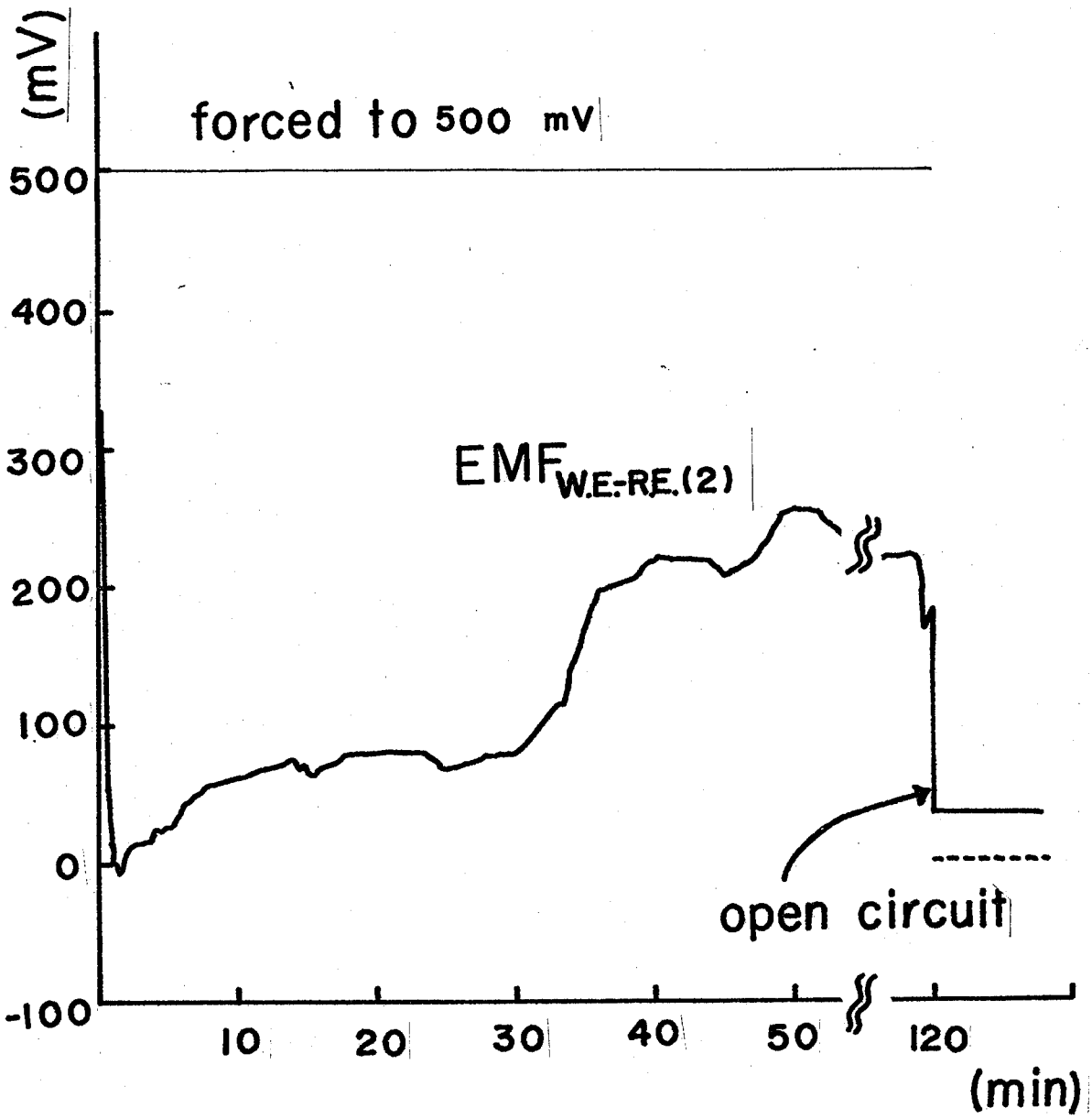

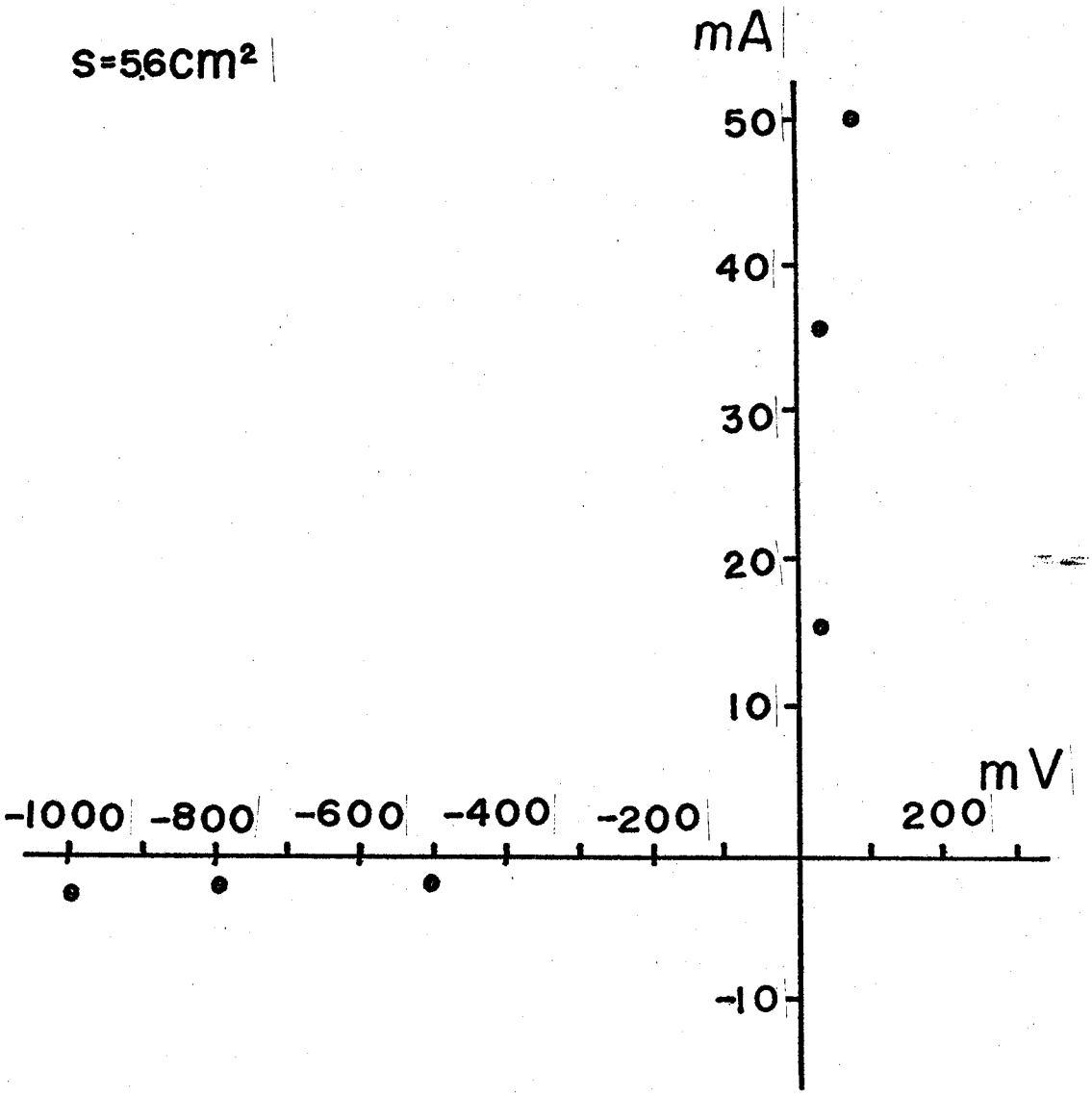

Figure 15. Current-voltage curve at Na_2O-$2SiO_2$ melt, 1052 °C.

Table 2. Electromotive force measurements for Oxygen concentration-overpotential in total voltage

Cathodic polarization

emf between W.E. & R.E(1)	emf between W.E. & R.E(2)	Temperature (°C)
-985	-902	1026
-585	-507	1026
-784	-682	1075
-484	-397	1075
-983	-909	1057
-986	-929	1057

IV EMF MEASUREMENTS FOR SOME BINARY OXIDE MELTS

IV-1 Preface

Binary mixtures like metal silicates, aluminates, germanates, borates, phosphates, titanates of various compositions and alkali fluoride-beryllium fluoride, provide a group of interesting liquid solutions which are realized only at high temperatures. They consist of net-work modifiers, or metal oxides, and of net-work formers, or acidic oxides, which consist of three dimentional net-works in liquid state. When the concentration of metal oxide, (or alkali fluoride in fluoride mixture) is very low, the net-work is modified only locally and the mixture is almost completely non-conductive[5,8,54]. With increase of metal oxide or alkali fluoride, the mixtures become electrolytic solutions, as the modification progresses and the net-work is broken into fragments of various sizes. After complete collapse of the net-work structure, they become so-called fused salts. With the increase of metal oxide, the viscosity decreases drastically on account of the collapse of the net-work structure and equivalent conductances increase monotonically from zero. Thus, these oxide mixtures change from covalent to ionic solution. This is not found in other mixtures at low

temperature or in general fused salts. Up to now, numbers of thermodynamic activities have been studied from theoretical as well as metallurgical view points. Previous theoretical treatments have devoted to the detailed caluculation of configurational entropy which arises from the modification of net-works. Such calculation have been consistent with experimental data as far as Gibbs free energy. However as partial molar enthalpies of $PbO-SiO_2$ [30], $PbO-B_2O_3$, alkali-borates [29] and $LiF-BeF_2$ [31], have been reported it became clear that the solutions were complex, especially so in the composition richer acidic oxide than 60 mol %. The informations of enthalpies and entropies are now indispensable to understand the properties of these solutions, the solvated state of ions, the inter-ion interaction, and the collapse of the net-work structure etc., in addition to spectroscopic and various kinetic data. Aluminates, titanates or silicates which have been studied most extensively are not appropriate to accomplish this goal, because these net-work structures grudually collapse in range of high acidic oxide concentration where the liquidus temperatures are too high to be studied in a Pt crucible. On the other hand germanates and borates are among the appropriate ones for this study. In the present study, relative thermodynamic quantites $\Delta\overline{G}$ of $Li_2O-B_2O_3$ melts, $\Delta\overline{G}$, $\Delta\overline{H}$, $\Delta\overline{S}$ of $Na_2O-B_2O_3$ and $K_2O-B_2O_3$ are measured. $\Delta\overline{G}$ of $Na_2O-P_2O_5$ melts are also measured,

though the other thermodynamic quantities were not obtained in high acidic oxide composition.

IV-2 Na_2O-P_2O_5 system

IV-2-1 Experimental

Activities of binary oxide mixture are interesting in two regions of composition. In dilute alkali oxide, the net-work modification is very local among the large frames of net-works. While in high alkali oxide concentration, the net-works have already been modified fairly well. In general, from phase diagram, oxide mixtures can not be studied for all of the composition region, except PbO-oxide melts, because of very high melting point or high volatility. The A_2O-P_2O_5 system is appropriate one to study in the region of 60 $\sim$ 30 mol % of alkali oxides.

The cell of the following type was constructed,

$$(Pt)O_2 \mid Na_2O\text{-}P_2O_5(I) \,\|\, Na_2O\text{-}P_2O_5(II) \mid O_2(Pt).$$

A virtual current from left to right in the cell is related to the electrode reaction,

$$\text{at the left electrode} \qquad O^{2-} = \frac{1}{2} O_2 + 2e$$

at the liquid junction $Na^+(I) = Na^+(II)$

at the right electrode $\frac{1}{2} O_2 + 2e = O^{2-}$

Where it is known that the transference number of Na^+ is unity at the liquid junction under the experimental condition. The emf of the cell, defined as the potential of the right electrode referred to that of the left electrode, is given by

$$E = \frac{1}{2F} RT \ln \frac{a_{Na_2O(I)}}{a_{Na_2O(II)}}$$

where the oxygen pressure at the two electrodes are equal. Schematic view of the cell is shown in Figure 16. The two oxide melts are separated by an alumina crucible in the bottom of which was a hole 0.3 mm in diameter. Bare platinum wires were used as electrodes. Operational details have been described in chapter II.

The chemical analysis was carried out for determination of the composition of samples by titration method with thimol blue and bromocresol green as indicators. The values, say, for sodium metaphosphate, $NaPO_3$ were 0.501, 0.490, 0.502 and 0.508 Na_2O mol fraction, for theoretical 0.500.

IV-2-2 Results and Discussion

Results are represented in Figure 17 and Table 3 at 800°C. Relative partial molar free energies of Na_2O changes linearly with X_{Na_2O} from 0.35 to 0.60. In spite of concentrated solution, as has been discussed previously in chapter II, the activity of Na_2O changes by as much as 10^3 with the change of 0.1 mole fraction of Na_2O. Kleppa et al. have reported the partial enthalpies of solution of solid WO_3 [81] in various Na_2O-P_2O_5 melt in Na_2O content from 50 to 60 mol %. According to the results, the partial enthalpies increase extremely near 50 mol % Na_2O, which suggests the partial enthalpy of Na_2O increase abruptly at this composition. The present results for relative partial molar free energies of Na_2O do not show such a change as the partial enthalpies.

IV-3 Li_2O-B_2O_3, Na_2O-B_2O_3 and K_2O-B_2O_3 systems

IV-3-1 Experimental

Cells of the following type were constructed,

$$\underset{\text{I}}{(Pt)O_2} \;\big|\; \underset{\text{II}}{A_2O\text{-}B_2O_3} \;\big\|\; \underset{\text{III}}{A_2O\text{-}B_2O_3} \;\big|\; \underset{\text{I}}{O_2(Pt)}$$

where A denotes lithium, sodium, or potassium. The broken lines denote the liquid junction, where two melts contact each other. As it been shown previously, the Pt-electrodes of both sides are reversible with respect to following reaction at equilibrium.

$$O^{2-} = \frac{1}{2} O_2 + 2e$$

The value of the liquid junction potential can be evaluated from

$$U_{ljp} = \frac{RT}{F_i} \sum \int \left(\frac{T_i}{Z_i}\right) d \ln a_i,$$

where F is the Faraday's constant and a_i, T_i, Z_i, are the activity, the transport number and the charge of i-th ion, respectively. As it is known that the transport number of A^+ is virtually unity, the electromotive force can be written as below:

$$E_{cell} = -\frac{RT}{2F} \ln a^{(III)}_{A_2O} / a^{(II)}_{A_2O}.$$

The Na_2O-$2B_2O_3$ melt was used as the reference melt for the Na_2O-B_2O_3 system, while 5 mol % A_2O-95 mol % B_2O_3 was used for the Li_2O-B_2O_3 and the K_2O-B_2O_3 systems. The relationship of emf and partial molar free energy is

$$\Delta\bar{G}_{A_2O} = -2FE_{cell} \ ,$$

and the general thermodynamic relation allows one to evaluate $\Delta\bar{H}_{A_2O}$ and $\Delta\bar{S}_{A_2O}$ from the temperature dependence of the E_{cell}.

The cell assembly is shown in Figure 18. It is composed of pairs of platinum crucibles, of Al_2O_3 tubes as insulators, and of Al_2O_3 boat. The Al_2O_3 rods and the Al_2O_3 boat constitute the liquid junction, when they were wetted with each melts on both sides. These components of the cell were assembled on an alumina brick, then they were all put into a stainless steel cup. A stainless steel tube was introduced between the furnace tube and the alumina reaction tube and was electrically grounded. Platinum wires of 1 mm diameter were used for the electrodes. The temperature was measured with a chromel-alumel thermocouple calibrated to the melting points of Zn, Pb, Al and NaCl. Temperature was maintained within ±1°C with a OHKURA EC 61 type controller. The emf was measured with a YOKOGAWA 2722 type potentiometer. The emf became constant after 12 hr after the cell was set up, and it remained constant for over one day.

All chemicals used were of the guaranteed reagent grade from WAKO PURE CHEMICAL INDUSTRIEDS, LTD. All of the glassy A_2O-B_2O_3 was prepared by melting anhydrous

alkali (Li, Na, K) carbonate and boric acid of desired compositions in an electric furnace in an air atomosphere at 950° ~ 1000°C for more than 20 hr. The melts were quenched to solid glass on a stainless steel plate. The concentrations of alkali metal ions in A_2O-B_2O_3 glasses were determined with a Hitachi 139 type flame photometer. The results indicated that the concentration change did not exceed ±0.3 mol % A_2O as compared with the initial compositions and the concentration was also found unchanged during the emf measurements. Therfore, the compositions below are derived from rations of weighted amounts of the chemicals.

IV-3-2 Experimental Results

The experimental data for Li_2O-B_2O_3, Na_2O-B_2O_3 and K_2O-B_2O_3 are given in Table 4, 5 and 6 respectively. For the melt of high alkali oxide compared to the reference solutions, the sign is negative, because of the higher tendency of discharge of O^{2-} on that side. The regression lines emf/mV on temperature are plotted in Figure 19 and 20.

The relative partial molar free energies of alkali oxides, $\Delta\bar{G}_{Li_2O}$, $\Delta\bar{G}_{Na_2O}$ and $\Delta\bar{G}_{K_2O}$ are shown in Figure 21, where the emf values of Na_2O-B_2O_3 system, like other

alkali borate, are plotted in reference to 5 mol % A_2O -95 mol % B_2O_3. The reason why we chose the reference melt of the composition not less than 5 mol % A_2O was to avoid the possible contribution to the conductance from the small amount of water present in low alkali melts. We do not show the regression lines of Li_2O-B_2O_3 system, since the stability of the emf values were not good enough to allow us to evaluate the temperature dependence. The lithium's attack on the Pt electrode is a probable cause, since we got consistent emf values of Li_2O-B_2O_3 when the electrode had been dipped and leached in B_2O_3 or Na_2O-$2B_2O_3$ melts for a day after the previous run. The emf was constant for only half a day. Therefore, we report the data of two or three separate runs of emf for lithium borate in Table 4. Emf data for alkali borate without temperature dependence have already been given by Stegmaier and Dietzel. The cells for sodium and potassium borate were constructed as an alkali oxide concentration cell in alkali borate, but for lithium borate it was not constructed like that because pure B_2O_3 liquid was selected as the reference. In Figure 21, Stegmaier and Dietzel's data with our old data are also given. The reference were 0.7 mol % and 0.56 mol % melts for Na_2O and K_2O respectively in Stegmaier and Dietzel's original data. However, the values are now plotted against 5 mol % A_2O-95 mol % B_2O_3 solution. We think

that the present data is the best of the three sets, because we eliminated the possible contribution to conductivity by water dissolved in borate melts* for low A_2O concentration and because we used Pt cells, which protect the melts from previous contamination with alumina crucible.

In Figure 22 we show the relative partial molar free energies of B_2O_3, $\Delta\bar{G}_{B_2O_3}$, which are obtained from $\Delta\bar{G}_{A_2O}$ with the Gibbs-Duhem relation. The precision of $\Delta\bar{G}_{B_2O_3}$ is better than ± 0.1 $kcal_{th}$ in the low composition range of A_2O. The activities of B_2O_3 in alkali borate, Ag_2O-B_2O_3, and PbO-B_2O_3 are plotted in Figure 23. In Figure 24 we show the relative partial molar enthalpies of Na_2O and K_2O, $\Delta\bar{H}_{Na_2O}$ and $\Delta\bar{H}_{K_2O}$ as well as the corresponding data from Østvold and Kleppa, where the original data of $\Delta\bar{H}_{B_2O_3}$ was transformed with Gibbs-Duhem

---

* Specific conductance of sodium borate prepared from boric acid and sodium carbonate in the same manner as the present melts were 6×10^{-3}, 1×10^{-3}, 8×10^{-4}, 8×10^{-5}, 5×10^{-5} $ohm^{-1}cm^{-1}$ at 5, 3, 1, 0.3, 0.1 mol % Na_2O-borate melts, respectively, at 900°C. This means conductance by H_2O can be neglected in the solution containing A_2O of more than 5 mol %, since the solubility of H_2O has the largest value in pure B_2O_3 melt[18].

relation and the reference was taken to 5 mol % A_2O-95 mol % B_2O_3 melt. In Figure 25, we give the $\Delta\overline{H}_{B_2O_3}$, which is determined from $\Delta\overline{H}_{Na_2O}$ and $\Delta\overline{H}_{K_2O}$, in parallel with Østvold and Kleppa's data. The precision of $\Delta\overline{H}_{B_2O_3}$ in reference to pure liquid B_2O_3 is ± 0.3 $kcal_{th}$ in the region of dilute alkali oxide composition.

In Figure 26 and 27, we give the relative partial molar entropy of A_2O, $\Delta\overline{S}_{A_2O}$, and the corresponding values of B_2O_3, $\Delta\overline{S}_{B_2O_3}$, is derived from $\Delta\overline{S}_{A_2O}$. The precision of $\Delta\overline{S}_{B_2O_3}$ is ± 0.5 cal_{th}/deg in dilute A_2O composition.

Finally in Table 7, 8 and 9, we represent the basic data of $\Delta\overline{G}_{A_2O}$, $\Delta\overline{H}_{A_2O}$ and $\Delta\overline{S}_{A_2O}$ in alkali borate melts, numerically. The precision of the data was estimated for each run in accordance with Doerffel's paper.

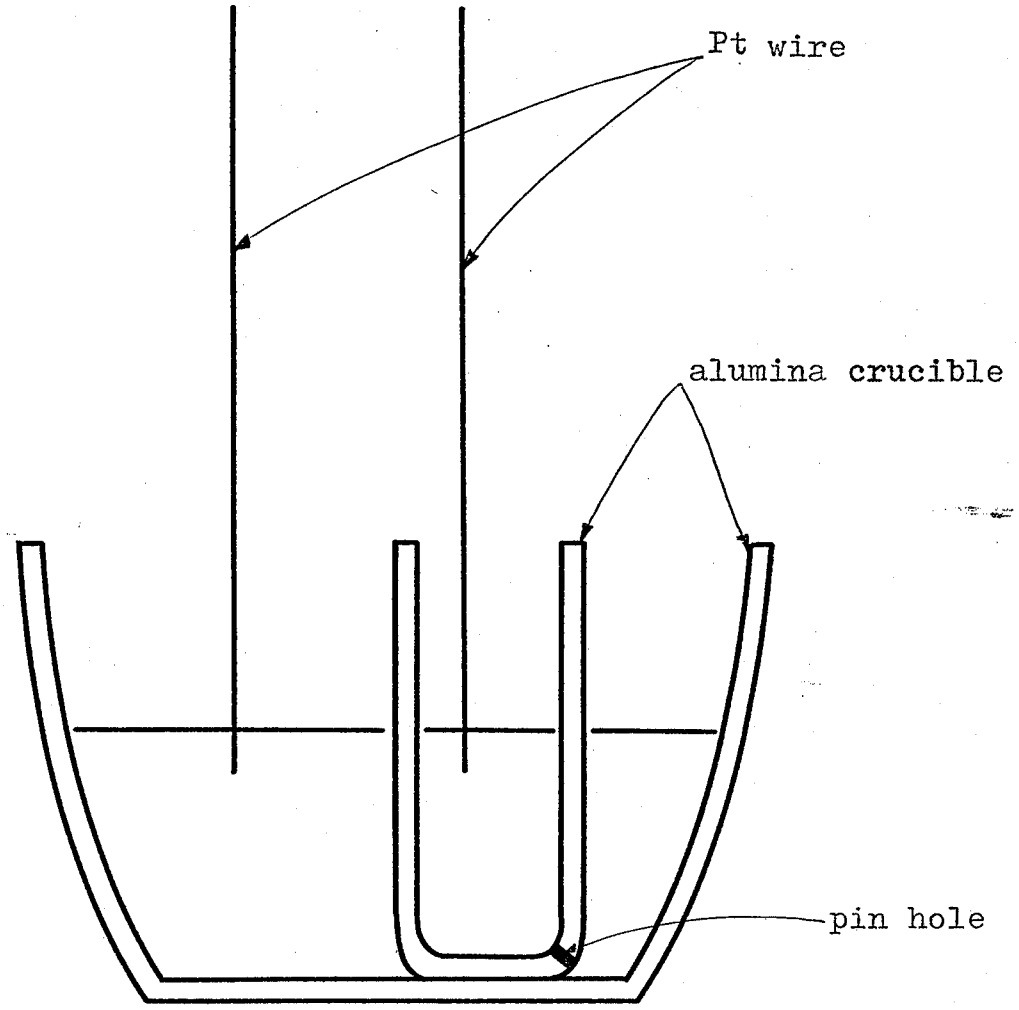

Figure 16. Cell assembly for emf measurements.

Figure 17. Relative partial molar free energies of Na_2O in Na_2O-P_2O_5 melts at 1073 K (Reference melt; X_{Na_2O}: 0.5)

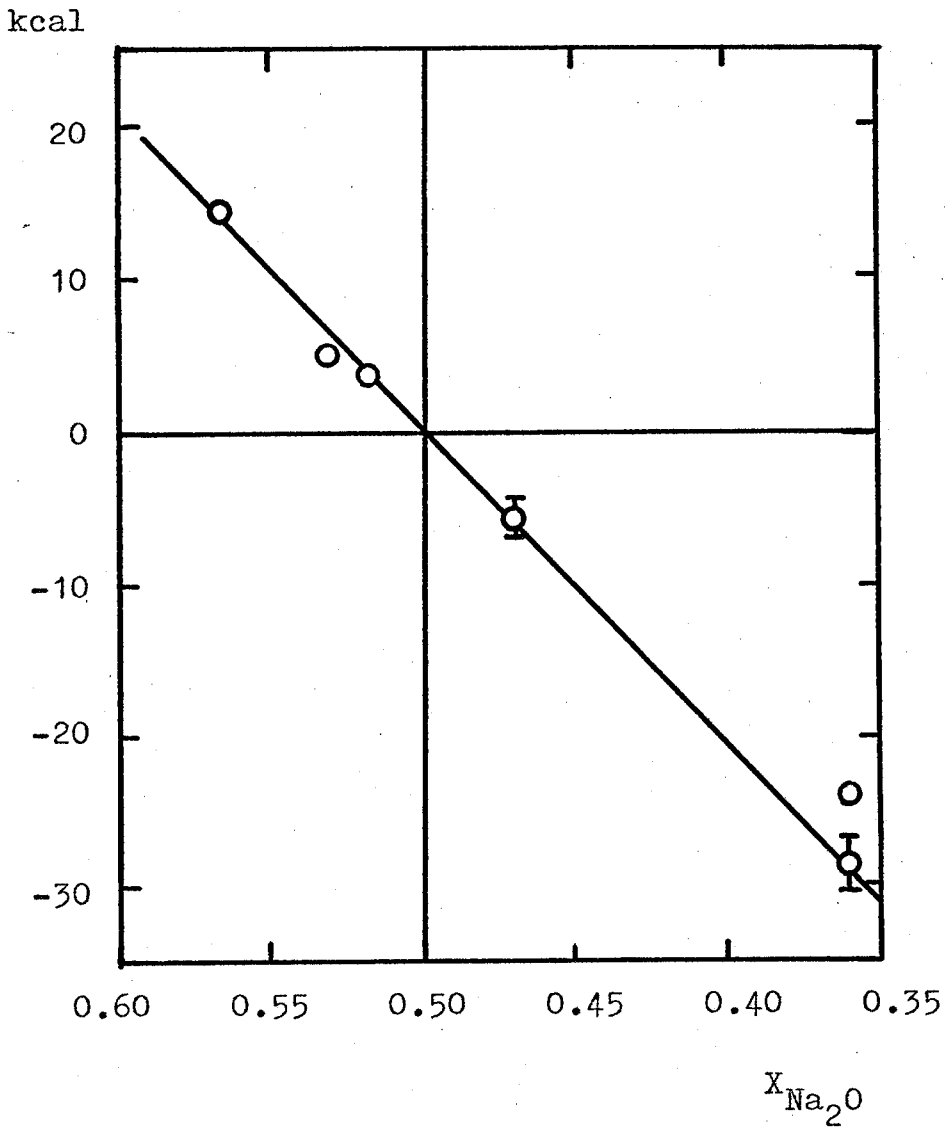

Figure 18. Cell assembly for emf measurement in alkali borate melt.

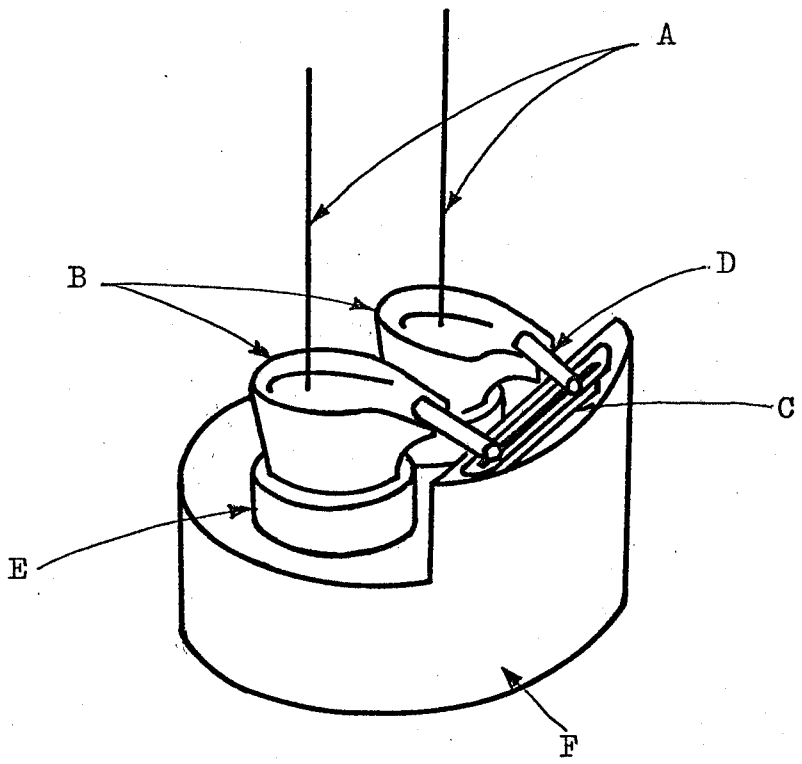

Figure 19. Temperature dependence of emf for $Na_2O-2B_2O_3$ melts
(reference melt: $Na_2O-2B_2O_3$)

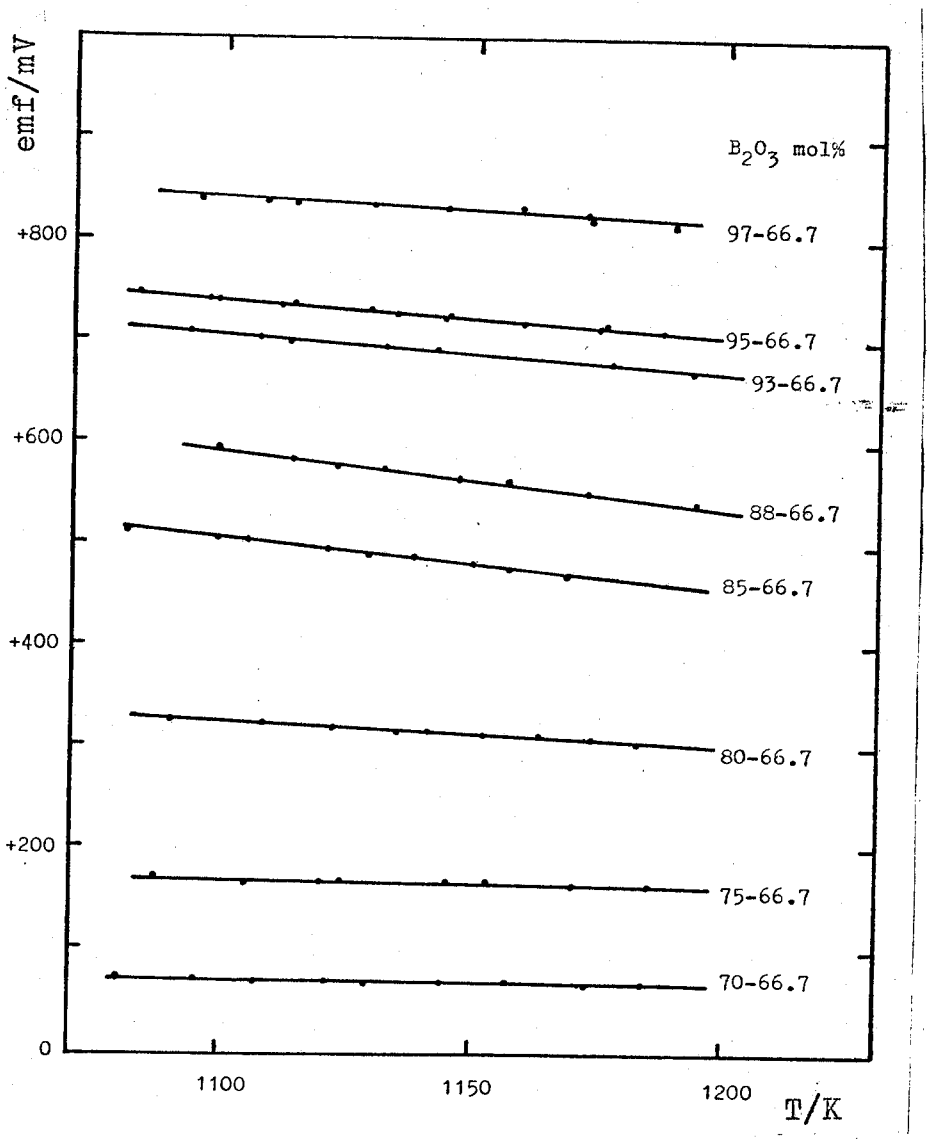

Figure 20. Temperature dependence of emf for K_2O-B_2O_3 melts (reference melt: 5 mol % K_2O-95 mol % B_2O_3).

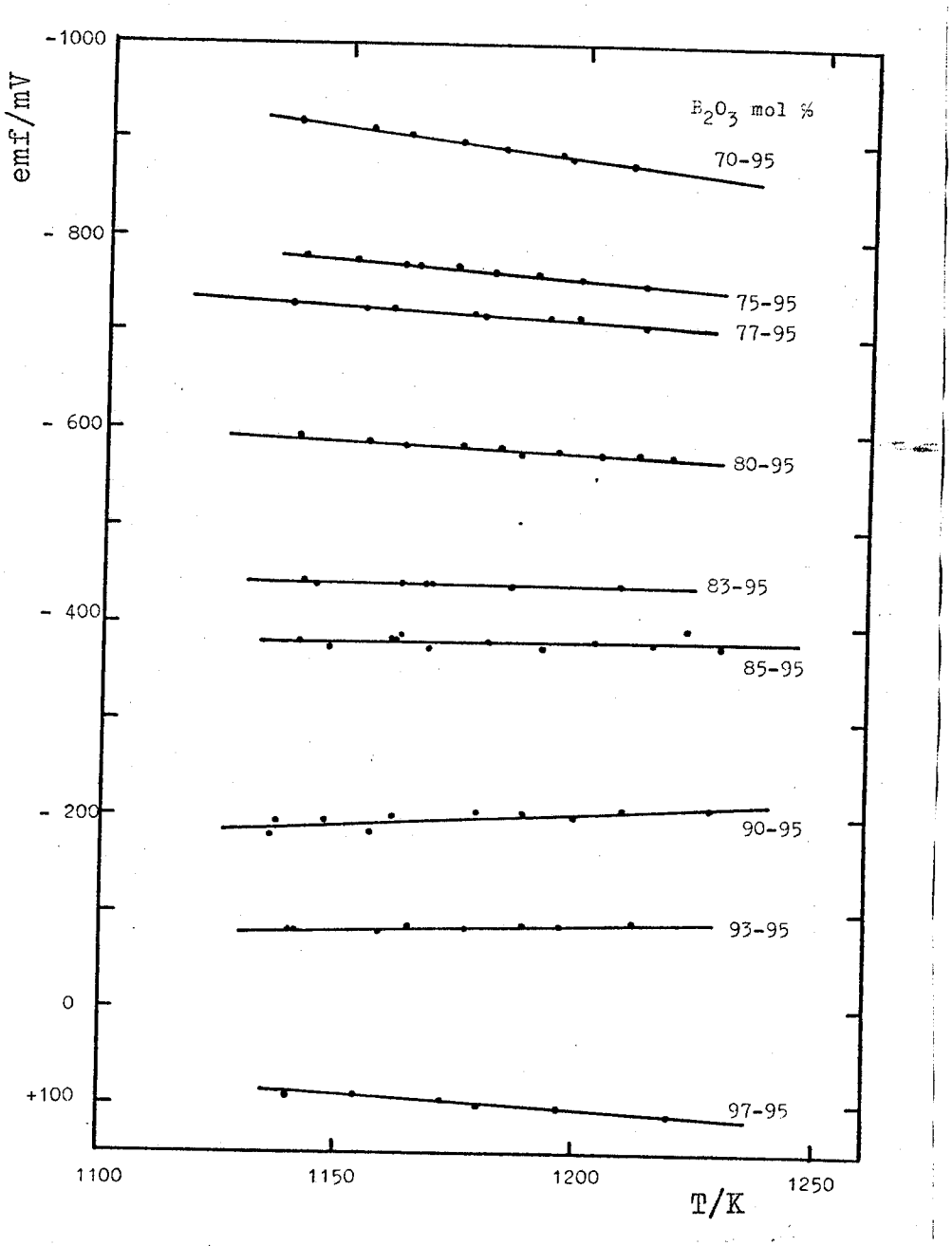

Figure 21. Relative partial molar free energies of alkali oxides in the alkali borate melts.

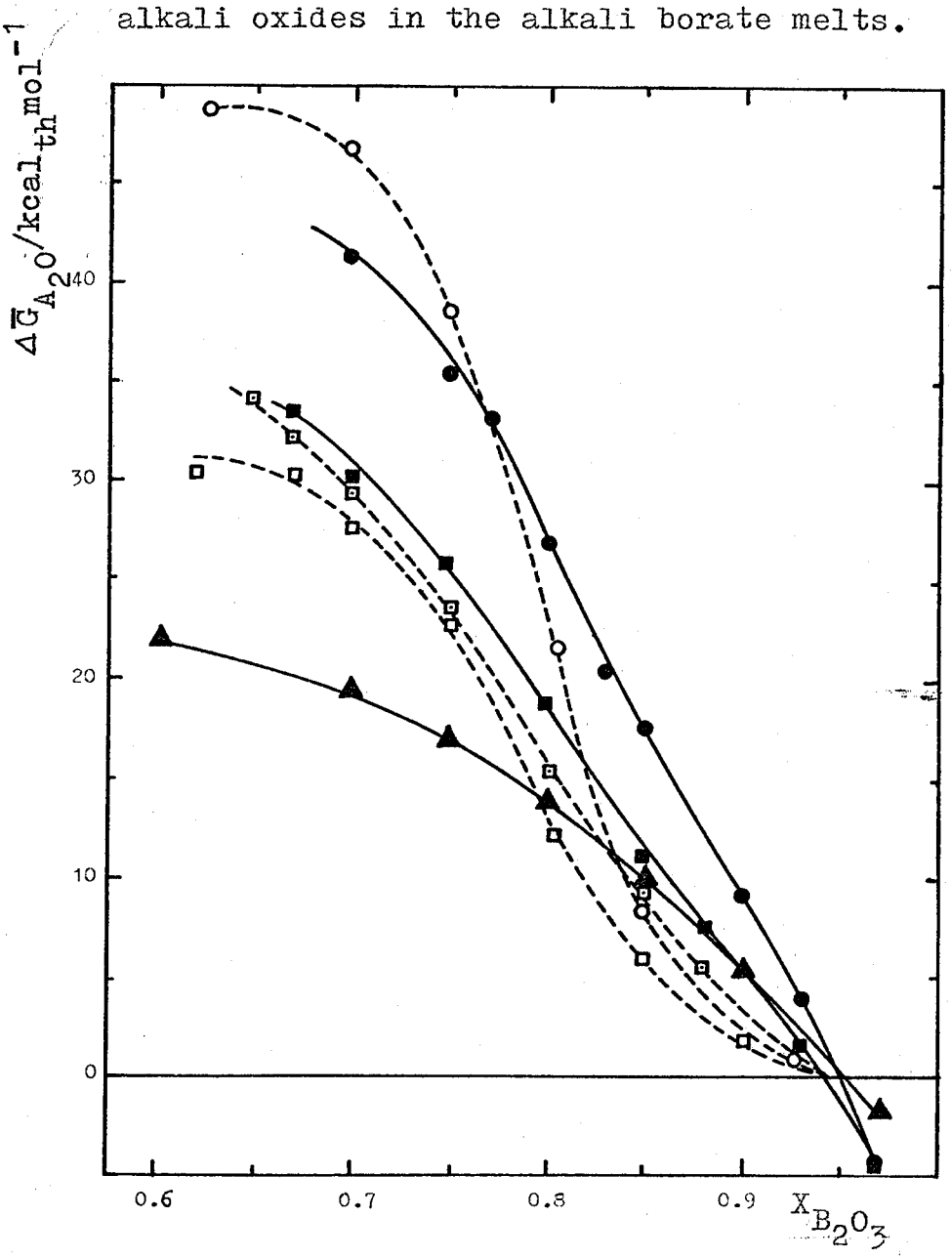

$\Delta\bar{G}_{Li_2O}$, $\Delta\bar{G}_{Na_2O}$ and $\Delta\bar{G}_{K_2O}$, referred to 5 mol % alkali oxide-95 mol % boron oxide melts at 1198 K, 1137 K, 1175 K respectively.

Li_2O-B_2O_3: ▲, this work. Na_2O-B_2O_3: ■, this work; ⊡, Sato et al. at 1123 K; □, Stegmaier et al. at 1123 K.

K_2O-B_2O_3: ●, this work; ○, Stegmaier et al. at 1123 K.

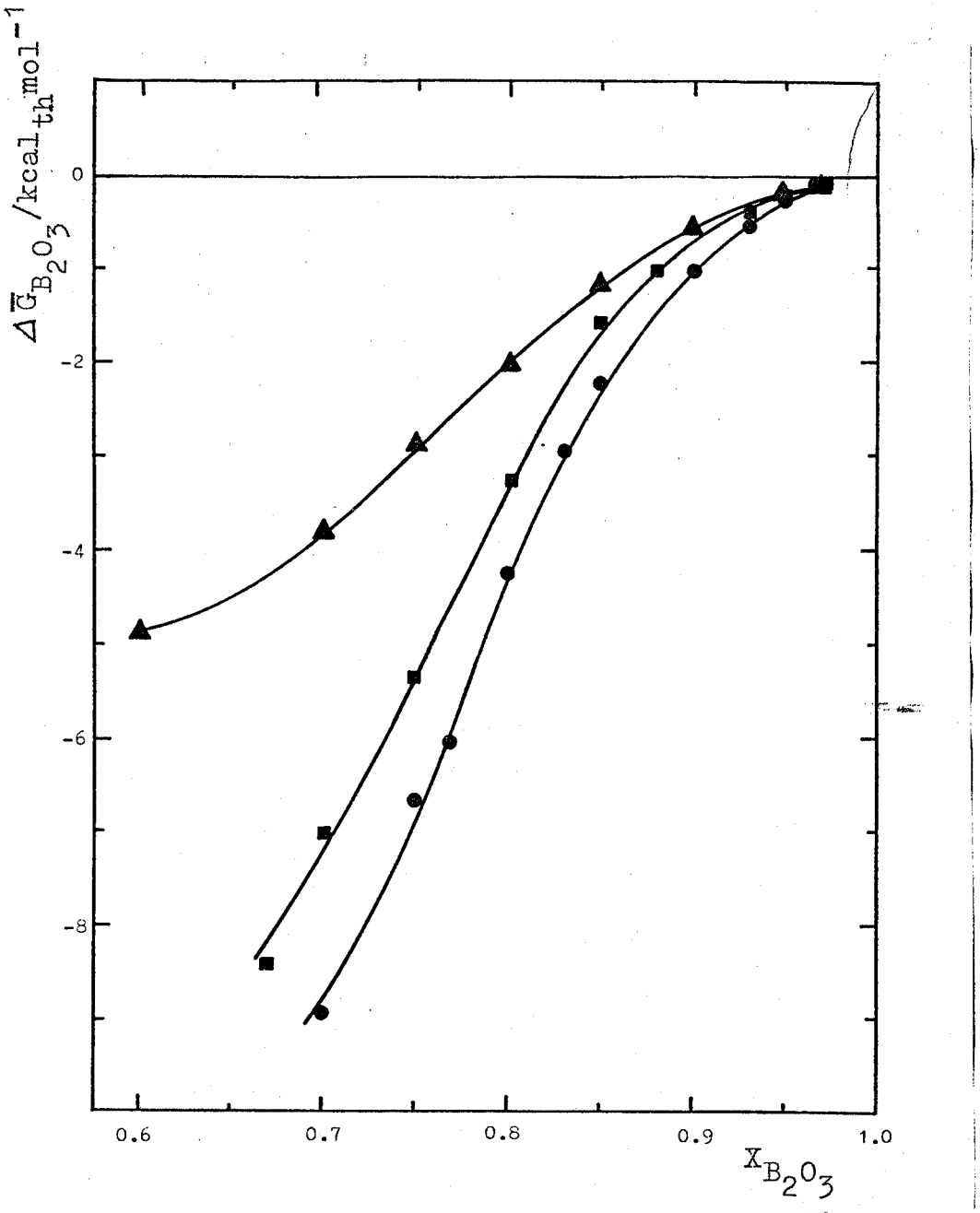

Figure 22. Relative partial molar free energies of B_2O_3, $\Delta\bar{G}_{B_2O_3}$, in the alkali borate melts.
Li_2O-B_2O_3: ▲, at 1198 K. Na_2O-B_2O_3: ■, 1137 K.
K_2O-B_2O_3: ●, at 1175 K.

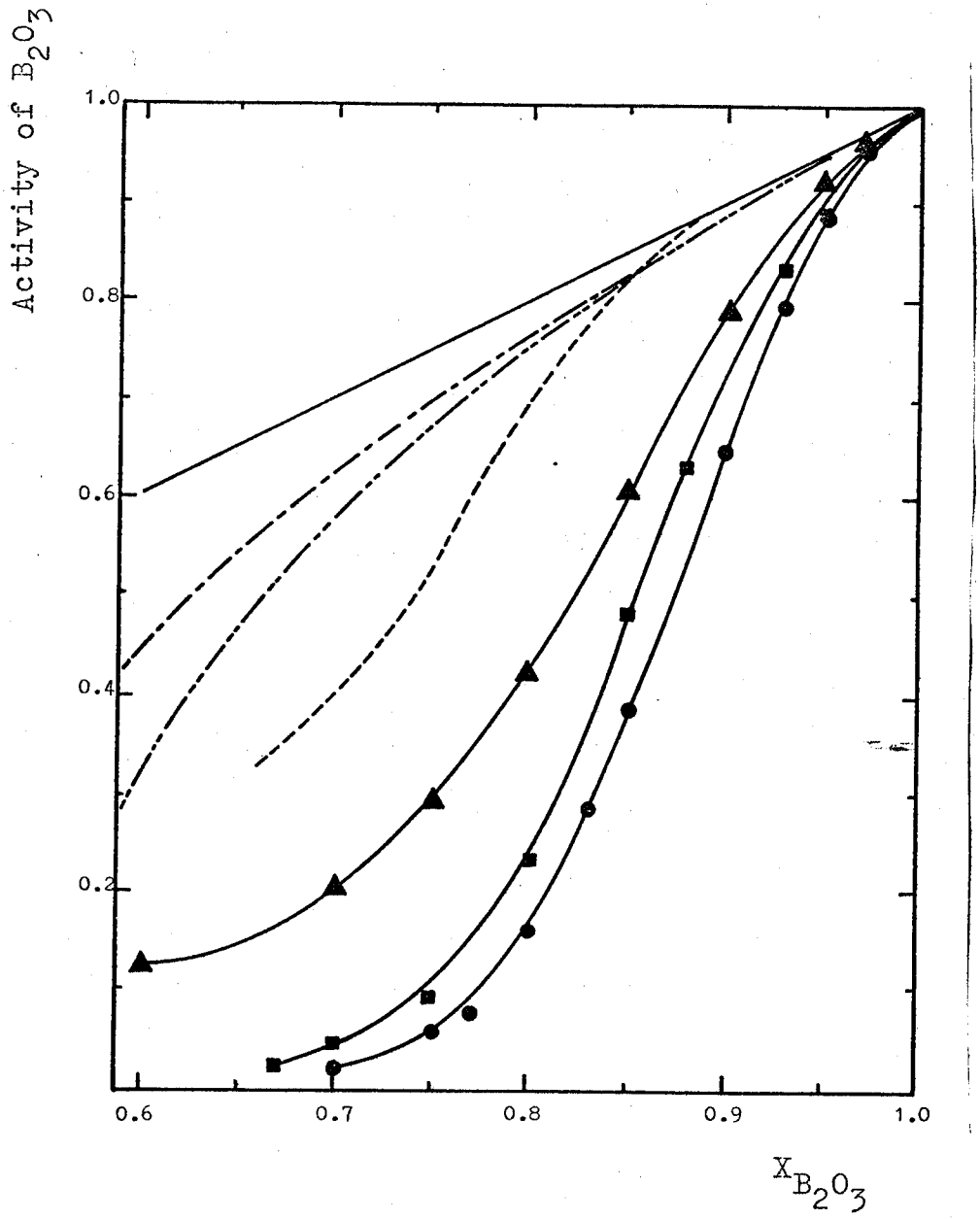

Figure 23. Activities of B_2O_3 in the alkali borate melts.
$PbO-B_2O_3$: ——·——, Sridhar et al. at 1273 K;
——·——, Lepinskikh et al. at 1273 K.
$Ag_2O-B_2O_3$: ------, Willis et al. at 1123 K.
$Li_2O-B_2O_3$: ▲, at 1198 K, $Na_2O-B_2O_3$: ■, at 1137 K,
and $K_2O-B_2O_3$: ●, at 1175 K, are present work.

Figure 24. Relative partial molar enthalpies of alkali oxide in the alkali borate melts (reference melts: 5 mol % alkali oxide-95 mol % boron oxide).

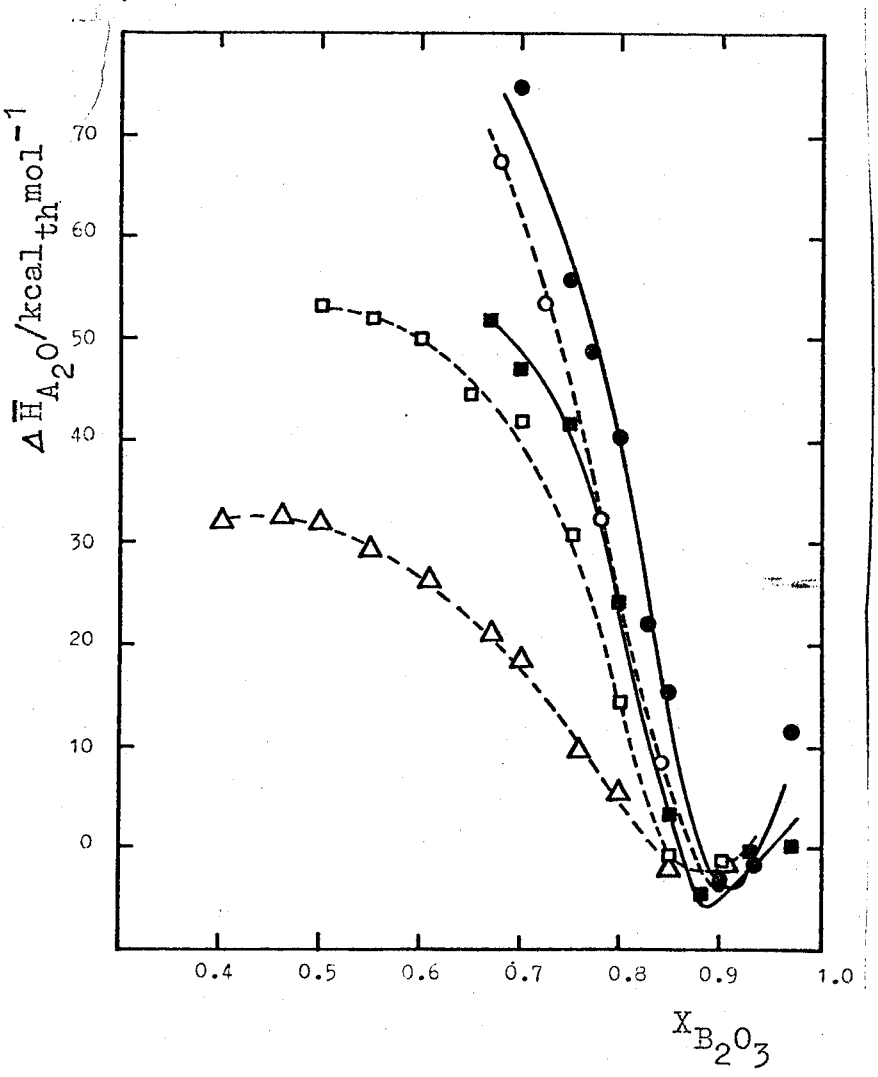

Li_2O-B_2O_3: △, from Ostvold et al. at 1213 K.

Na_2O-B_2O_3: ■, this work, at 1137 K; □, from Ostvold et al. at 1258 K.

K_2O-B_2O_3: ●, this work, at 1175 K; ○, from Ostvold et al. at 1258 K.

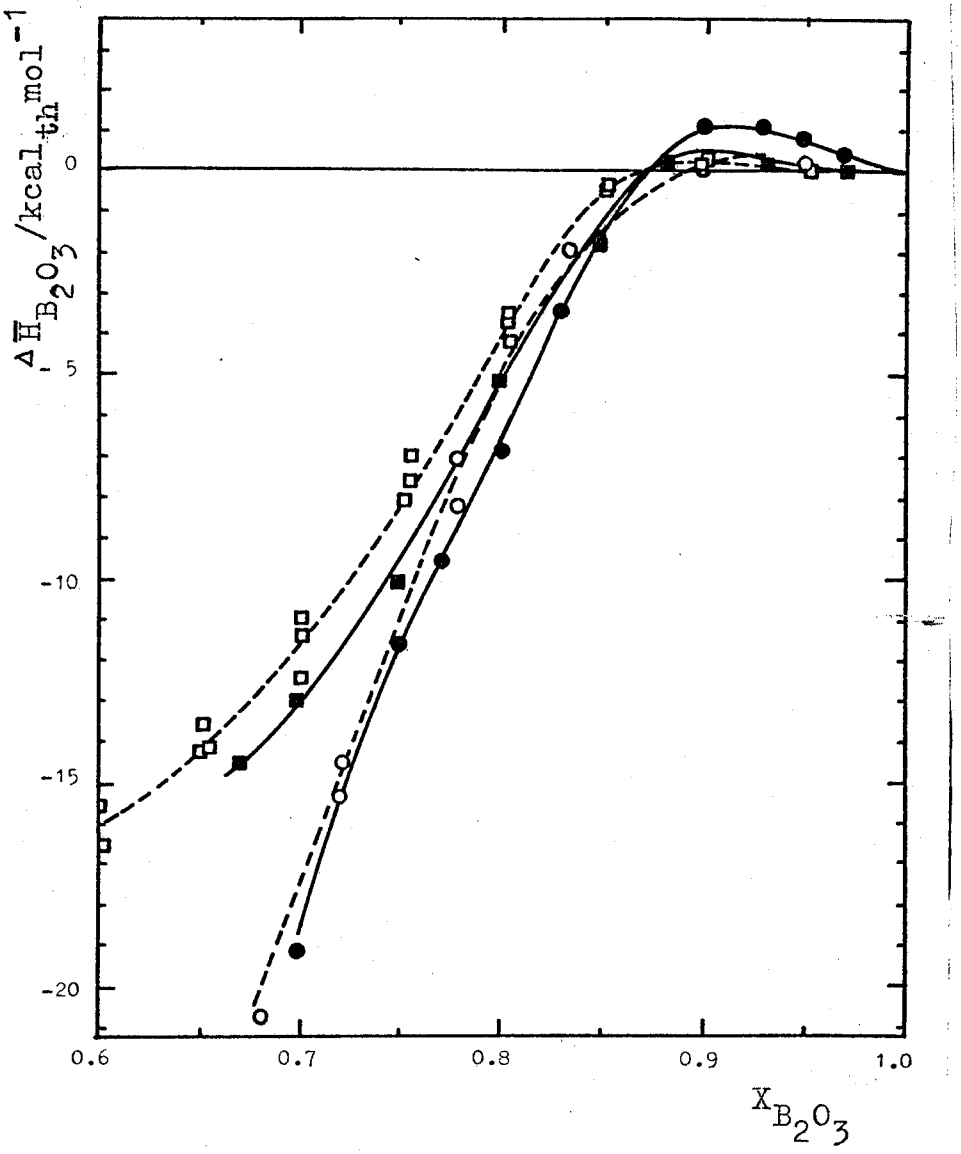

Figure 25. Relative partial molar enthalpies of B_2O_3 in Na_2O-B_2O_3 and K_2O-B_2O_3 melts. Na_2O-B_2O_3: ■, this work at 1137 K; □, Ostvold et al. at 1258 K. K_2O-B_2O_3: ●, this work at 1175 K; ○, Ostvold et al. at 1258 K.

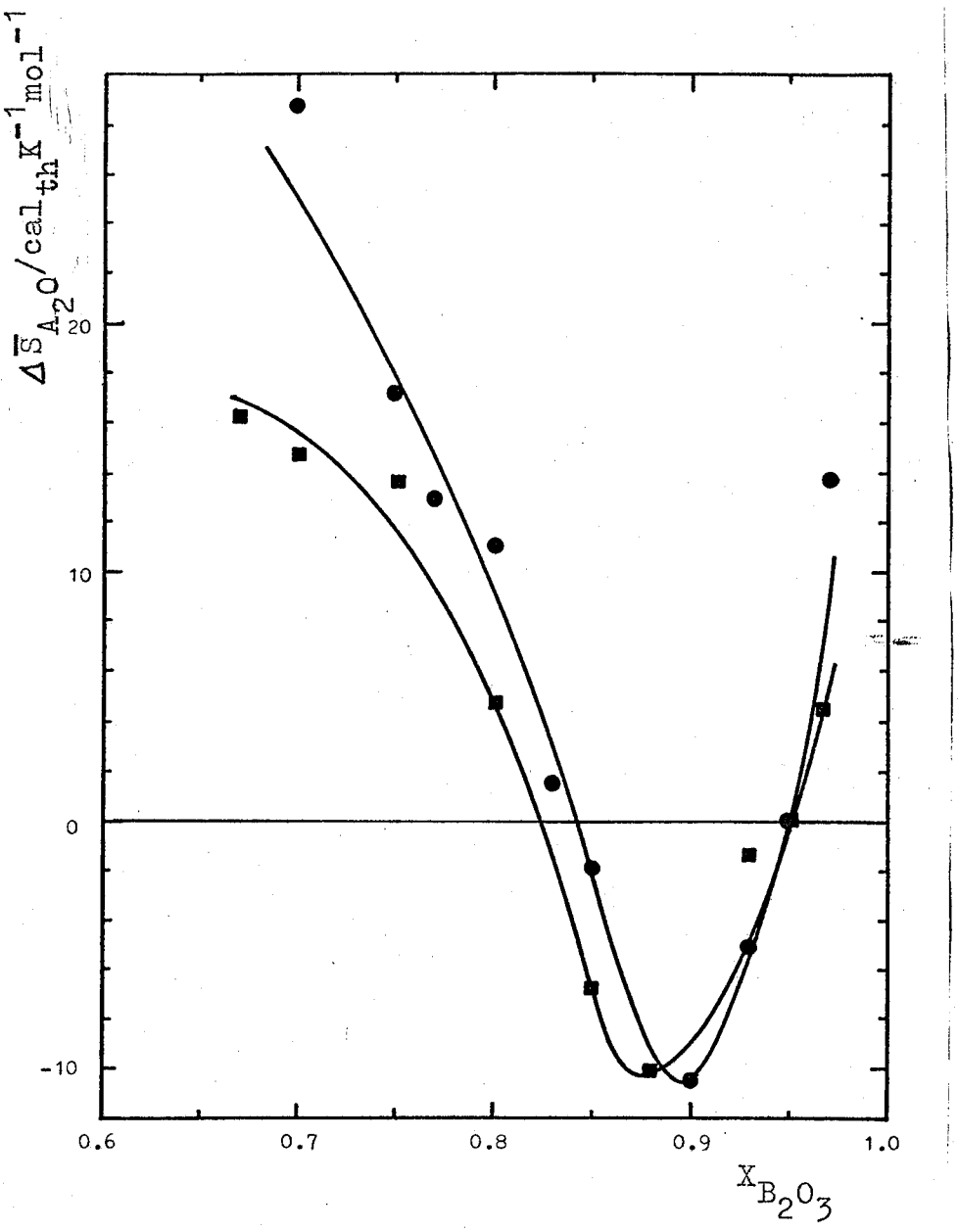

Figure 26. Relative partial molar entropies of alkali oxide in Na_2O-B_2O_3 and K_2O-B_2O_3 melts (reference melt: 95 mol % B_2O_3 solution). ■, Na_2O, at 1137 K; ●, K_2O-B_2O_3, at 1175 K.

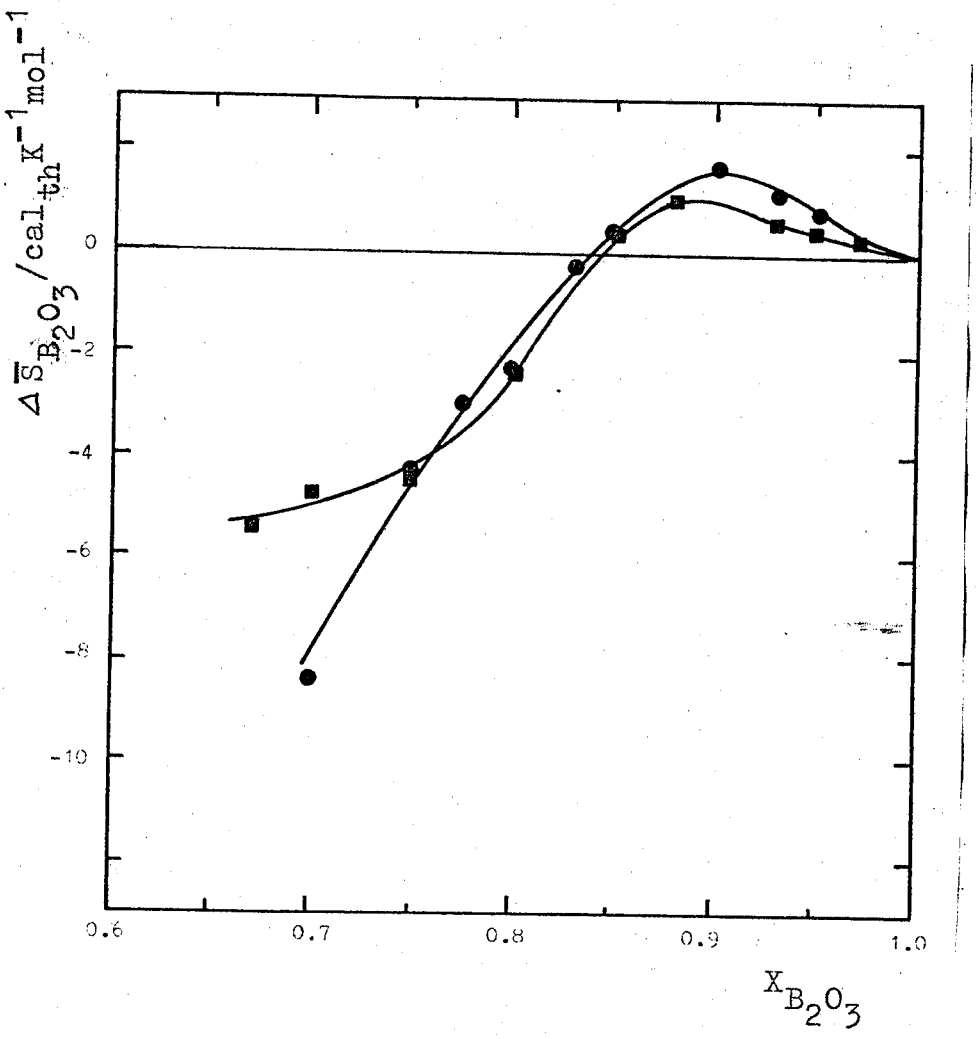

Figure 27. Relative partial molar entropies of B_2O_3 $\Delta\bar{S}_{B_2O_3}$ in Na_2O-B_2O_3 and in K_2O-B_2O_3 melts at 1137 K and 1175 K respectively, ■, Na_2O-B_2O_3; ●, K_2O-B_2O_3.

Table 3. EMF values in Na_2O-P_2O_5 melts at 1073 K

(Reference melt; X_{Na_2O}: 0.5)

(mV)		(Na_2O mol%)		(kcal)
113 ± 3		53.0		5.21 ± 0.14
82 ± 4		51.7		3.78 ± 0.18
315 ± 5		56.5		14.52 ± 0.23
121 ± 10		47.0		5.58 ± 0.46
510 ± 4	}	36 ± 1 mol%	{	23.52 ± 0.20
610 ± 40				28.13 ± 1.84

Table 4.

EMF values in Li_2O-B_2O_3 melts at 1198 K

(Reference melt; 5 mol% Li_2O - 95 mol% B_2O_3)

B_2O_3 mol%	EMF/mV
97	47
95	0
90	124, 137
85	217
80	301, 266, 274
75	365, 335
70	397, 383
60	461

Table 5. Temperature dependence of EMF in Na_2O-B_2O_3 melts (Reference melt; $Na_2O \cdot 2B_2O_3$).

B_2O_3 mol%	T/K	EMF/mV	B_2O_3 mol%	T/K	EMF/mV
97	1173	819.2	93	1142	692.0
	1189	815.0		1113	699.8
	1144	831.0		1093	710.9
	1114	837.7		1107	704.7
	1095	841.6		1132	694.8
	1108	837.3		1177	679.9
	1129	835.5		1193	669.0
	1172	826.1	88	1173	551.3
	1159	833.2		1147	564.4
95	1099	739.2		1123	577.7
	1114	735.0		1099	590.8
	1129	730.0		1114	583.2
	1145	724.9		1132	573.7
	1160	716.4		1157	560.1
	1176	714.5		1194	536.1
	1187	709.3	85	1157	475.9
	1176	714.5		1138	487.8
	1160	715.5		1121	495.2
	1144	721.1		1099	506.1
	1134	725.5		1081	512.4
	1111	733.0		1105	503.6
	1097	738.4		1129	490.9
	1083	747.3		1150	480.7
				1169	470.2

(continued) (Na_2O-B_2O_3)

B_2O_3 mol%	T/K	EMF/mV	B_2O_3 mol%	T/K	EMF/mV
80	1141	316.8	70	1173	64.4
	1163	312.0		1184	67.0
	1182	303.5		1157	68.6
	1152	311.8		1144	67.8
	1122	319.5		1121	67.6
	1090	327.5		1095	69.2
	1108	323.1		1081	70.0
	1135	317.0		1107	68.0
	1173	307.6		1129	66.2
75	1105	163.5			
	1145	166.3			
	1170	163.8			
	1185	162.4			
	1153	166.0			
	1120	167.7			
	1087	170.3			
	1124	165.5			

Table 6. Temperature dependence of EMF in K_2O-B_2O_3 melts (Reference melt; 5 mol% K_2O - 95 mol% B_2O_3).

B_2O_3 mol%	T/K	EMF/mV	B_2O_3 mol%	T/K	EMF/mV
97	1154	89.4	90	1137	-195.2
	1172	96.8		1161	-200.4
	1197	105.2		1179	-205.2
	1220	110.8	85	1204	-384.0
	1180	101.9		1169	-377.0
	1140	92.1		1148	-376.1
93	1141	- 79.7		1193	-377.6
	1159	- 82.0		1230	-379.4
	1177	- 83.8		1216	-382.3
	1197	- 86.3		1181	-383.0
	1212	- 89.3		1161	-386.4
	1189	- 87.2		1142	-383.2
	1165	- 85.7		1162	-385.9
	1141	- 82.7		1223	-395.4
90	1136	-180.3		1163	-390.0
	1157	-185.0	83	1163	-441.6
	1200	-199.6		1145	-442.6
	1228	-208.2		1169	-442.9
	1210	-207.6		1186	-441.5
	1189	-205.7		1209	-441.6
	1147	-197.3		1168	-443.9
				1143	-444.7

(continued) (K_2O-B_2O_3)

B_2O_3 mol%	T/K	EMF/mV	B_2O_3 mol%	T/K	EMF/mV
80	1187	-576.3	75	1181	-765.6
	1204	-575.7		1162	-772.4
	1219	-575.1		1141	-779.6
	1195	-578.2		1165	-770.2
	1183	-581.5	70	1140	-919.5
	1163	-587.2		1155	-911.3
	1141	-593.1		1174	-899.4
	1155	-589.5		1195	-885.6
	1175	-586.3		1210	-875.5
	1212	-577.5		1197	-882.3
77	1199	-718.2		1183	-893.6
	1177	-721.7		1163	-906.3
	1154	-727.2			
	1139	-731.1			
	1160	-726.3			
	1179	-721.3			
	1193	-717.0			
	1213	-708.0			
75	1152	-776.4			
	1173	-771.2			
	1190	-762.4			
	1213	-752.4			
	1199	-758.1			

Table 7. Experimental results for alkali borate melts

(cal_{th} = 4.184 J)

Li_2O-B_2O_3 melts at 1198 K

B_2O_3 mol%	$\Delta\bar{G}_{Li_2O}$ / $kcal_{th}mol^{-1}$
97.0	- 1.8
95.0	0
90.0	5.4
85.0	9.9
80.0	14.0
75.0	16.8
70.0	19.4
60.0	21.3

(± 1.5 kcal)

Table 8. Experimental results for alkali borate melts

(cal_{th} = 4.184 J)

Na_2O-B_2O_3 melts at 1137 K

B_2O_3 mol%	$\Delta\bar{G}_{Na_2O}$ / $kcal_{th}mol^{-1}$	$\Delta\bar{S}_{Na_2O}$ / $cal_{th}K^{-1}mol^{-1}$	$\Delta\bar{H}_{Na_2O}$ / $kcal_{th}mol^{-1}$
97.0	- 4.90 ± 0.17	4.5 ± 1.8	0.3 ± 2.2
95.0	0	0	0
93.0	1.53 ± 0.09	- 1.5 ± 1.0	- 0.1 ± 1.2
88.0	7.18 ± 0.06	-10.4 ± 0.7	- 4.6 ± 0.8
85.0	11.03 ± 0.06	- 6.8 ± 0.7	3.3 ± 0.8
80.0	18.89 ± 0.06	4.7 ± 0.7	24.3 ± 0.8
75.0	25.84 ± 0.09	13.7 ± 1.1	41.4 ± 1.3
70.0	30.38 ± 0.06	14.7 ± 0.6	47.1 ± 0.7
67.0	33.48 ± 0.09	16.2 ± 0.8	51.9 ± 1.0

Table 9. Experimental results for alkali borate melts

(cal_{th} = 4.184 J)

K_2O-B_2O_3 melts at 1175 K

B_2O_3 mol%	$\Delta\overline{G}_{K_2O}$ / $kcal_{th}mol^{-1}$	$\Delta\overline{S}_{K_2O}$ / $cal_{th}K^{-1}mol^{-1}$	$\Delta\overline{H}_{K_2O}$ / $kcal_{th}mol^{-1}$
97.0	- 4.55 ± 0.13	13.8 ± 2.1	11.6 ± 2.5
95.0	0	0	0
93.0	3.91 ± 0.07	- 5.1 ± 1.0	- 2.0 ± 1.2
90.0	9.16 ± 0.30	-10.5 ± 3.1	- 3.1 ± 4.0
85.0	17.67 ± 0.27	- 1.9 ± 3.1	15.5 ± 3.9
83.0	20.42 ± 0.05	1.6 ± 0.9	22.3 ± 1.1
80.0	26.94 ± 0.11	11.2 ± 1.4	40.1 ± 1.8
77.0	33.29 ± 0.09	13.0 ± 1.3	48.5 ± 1.6
75.0	35.40 ± 0.06	17.2 ± 0.9	55.7 ± 1.1
70.0	41.42 ± 0.05	28.6 ± 0.8	75.0 ± 1.0

V GENERAL DISCUSSION FOR THE RESULTS OF THIS STUDY

Up to this time, many experiments and discussions have been carried out for binary oxide mixtures from both kinetics and thermostatics. From the view point of kinetics, mostly from viscosity measurements, it has been clearified that the net-work structures of pure acidic oxide are retained in liquid state and with addition of metallic oxide, net-work modification initiates and progresses to end up finally with ionic mixture like fused salts. Corresponding to such change of concentration, the equivalent conductance of cation increases monotonously[5,8]. This behavior of the conductivity have been explained from the considerable increment of the viscosity of oxide melt by Bockris et al.[3] and by Riebling et al.[7] Also from the viscosity measurements, the anion models have been proposed and have contributed to the development of oxide mixtures. On the other hand, from the view point of thermodynamics, many discussions have been carried out about the activities of oxide melts. This explanation is very valuable in relation to basicities or reactivities of them. Based on their results, many studies have been devoted to the estimation of the distribution of silicate anions which have become so detailed as to the discussion of the type of side chains. In these treatments, the

equilibrium constant for net-work modification is assumed to be unchanged over all composition and the partial molar enthalpies or excess entropies of the components have not been discussed. In spite of such a simple hypothesis, in fact, the experimental data for thermodynamic activity can be reproduced fairly well. This treatment is now commonly accepted for oxide mixtures at high temperatures.

The behaviors of the binary oxide mixtures that have been disclosed in the present study show that $\Delta\bar{H}$ and $\Delta\bar{S}$ of both components are not so simple. In Figure 24, $\Delta\bar{H}_{A_2O}$ in alkali borate decreases for concentration from 100 to 85 mol % B_2O_3, which correspond to the positive relative partial enthalpies of B_2O_3. The partial enthalpy of a component must increase monotonously with increase of the concentration from the infinite dilution to the pure substance, if the mixture is regular[82]. The same behavior of enthalpies as $\Delta\bar{H}_{A_2O}$ can be seen also in Ag_2O-B_2O_3[16], where $\Delta\bar{H}_{Ag_2O}$ decreases steadily from 100 to 70 mol % B_2O_3 by more than 25 kcal. Such phenomena are observed also in LiF-BeF_2, KF-BeF_2[31] and Na_2O-GeO_2[55] systems. On the other hand, the change of $\Delta\bar{S}_{A_2O}$ with composition of alkali borate is also not so simple as we expect in a regular solution as is shown in Figure 26. These interesting behaviors, which can not be found in other fused salt mixtures, seem to appear generally only in a series of mixtures including net-work forming and

net-work modifing substances at the same time. On the other hand, in the composition range from 85 to 70 mol % B_2O_3, $\Delta\overline{H}_{A_2O}$, $\Delta\overline{S}_{A_2O}$ in alkali-borate melt increases severely as much as 50 ~ 70 kcal, and 30 ~ 40 e.u. respectively. The present author would like to explain these behaviors in the following discussion.

With respect to A_2O-B_2O_3 and A_2O-GeO_2 system, the experiments are comparatively easy in high acidic oxide composition because of the low liquidus and nonvolatility[56]. If the alkali oxide completely dissociate in the melt, the inter-ion distance is 8.4 Å from molar volume data at 3 mol % of Na_2O in sodium borate. If the alkali ions are in ion pair with oxygen, the mean inter-pair distance is 10.6 Å, at the same composition. In the case of higher association, the corresponding distance will become longer. In spite of such a long distance, the relative partial molar enthalpies of A_2O do change with composition definitely. This means the type of interaction between neighboring alkali oxide in solution should be not of short range but of long range, that is, coulombic interaction.

The viscosities and the conductivities in both oxide system have already been known. In A_2O-GeO_2 system, the viscosity decreases extremely by net-work modification in the composition range from 0 to 30 mol % A_2O[7]. Thus, $\log(\eta_{soln}/\eta_{GeO_2}) \cong -4$. In A_2O-B_2O_3 system,

the viscosities vary scarcely[5] , compared with A_2O-GeO_2 system, because of the formation of four-fold coordination[57]. From 800 to 900°C, there lie regions where the viscosity decreases initially, then increases oppositely, because of net-work modification and four-fold coordination, respectively and at last decrease again because of net-work modification. In spite of these two different behaviors of A_2O-GeO_2 and A_2O-B_2O_3, the equivalent conductances of alkali ion in both systems decrease[5,8] monotonously toward zero, from 30 mol % A_2O to the pure GeO_2 or B_2O_3. This suggests the viscosity does not contribute to the equivalent conductance. The ionic state in solution seems to control the conductivity in both A_2O-B_2O_3 and A_2O-GeO_2 systems. That is to say, ionic state changes gradually with decrease of the A_2O concentration.

The dielectric constant at high temperature has been measured directly by means of microwave absorption[58], whose value in Na_2O-B_2O_3 is only about 5 at 5 mol % Na_2O. Therefore, even if ions are solvated in dissociated state, the solvation energy by Born's equation[59] are considered to be small. Completely dissociated state is considered not to be stable, especially in dilute solution of A_2O.

Ag_2O-B_2O_3 and H_2O-B_2O_3 systems can be seen to form ionic association from solubility measurement, though the type of the state of silver or hydrogen ion in solution are not always same as alkali ion. Hennessy

et al.[16] measured the solubility of Ag_2O in Ag_2O-B_2O_3

$$Ag_2O \text{ (in borate)} = 2\,Ag + \frac{1}{2}O_2.$$

The result showed for mixtures high in B_2O_3 the Ag_2O content was found to be proportional to the square root of the oxygen pressure. This means that when Ag_2O is dissolved in B_2O_3, the two silver ions and the borate groups formed can be discribed as an undissociated complex[60]. The experimental results were also ascertained by Maekawa et al.[17] Franz measured the solubility of H_2O in H_2O-B_2O_3 system[18].

$$H_2O \text{ (borate)} = H_2O \text{ (gas)}$$

H_2O content was found to be proportional to the square root of the pressure of H_2O. This means the H_2O dissolved as an ion pair like $>B\text{-}O^{\delta-}\text{-}H^{\delta+}$. Kodama et al. have measured the conductance of both Ag_2O-B_2O_3[61] and H_2O-B_2O_3[62,63] systems. The data, in each system, represent the monotonous decrease of equivalent conductance with decrease of A_2O concentration, just like that of alkali borate or germanate melts.

Further, under high pressure and high temperature molar conductivities are measured in $HgCl_2$, $HgBr_2$, HgI_2 and $BiCl_3$ by Tödheide et al.[64,65] The ionic conductivities

decrease monotonously with decrease of density. This behavior is explained by the notion that the ionic association propagates continuously with decrease of density[66,67,68]. Their activation energies are very large as much as those of alkali borate[5] or alkali germanate[8] in high acidic oxide composition, differing from the value in common fused salts[69,70].

From these behaviors of alkali ion in borate or germanate, author considers that alkali ion especially in dilute A_2O concentration, exists in associated state such as ion pair and gradually dissociate with increment of alkali oxide.

As the A_2O concentration increases from the infinite dilution, the ion pairs, i.e. the electric dipoles should begin to interact with each other. Haskell has calculated dipole-dipole and dipole-induced dipole interaction excluding the association and dispersion force for ethanol-heptan system[71], assuming the Onsager's equation for dielectrics. The curves of $\Delta\bar{H}_{ethanol}$ and $\Delta\bar{S}_{ethanol}$ from the result bears remarkable resemblance to our $\Delta\bar{H}_{A_2O}$ and $\Delta\bar{S}_{A_2O}$ curves for concentrations from 100 to 90 B_2O_3 mol %. These similarities of $\Delta\bar{H}_{A_2O}$, $\Delta\bar{S}_{A_2O}$ are also found in Ag_2O-B_2O_3, LiF-BeF_2, KF-BeF_2 and Na_2O-GeO_2. Thus in addition to the previous kinetic information, this equilibrium discussion also suggest ionic pair formation in acidic oxide-rich composition.

In order to ascertain whether actually the dipole-dipole interaction in oxide mixture can give the same order of the magnitude of the energy of mixing, the present author calculated approximately the dipole-dipole interaction with Onsager's equation for dielectrics in accordance with Haskell's treatment.

Borate or germanate melts are not necessarily appropriate for this type of research, because in these systems several compounds are known in solid phases and change of co-ordination number of oxygen around metal ions from 3 to 4 and 4 to 6 occurs in borate and in germanate, respectively. The more appropriate systems to be considered, are alkali fluoride-beryllium fluoride systems. Especially LiF-BeF_2 is only one system where the relative partial molar quantities, $\Delta\bar{G}$, $\Delta\bar{H}$, $\Delta\bar{S}$ are known in all range of composition[31,72,73]. The corresponding integral quantities with composition are shown in Figure 28 where $\Delta\bar{H}_{LiF}$, $\Delta\bar{S}_{LiF}$ behave just like $\Delta\bar{H}_{A_2O}$ and $\Delta\bar{S}_{A_2O}$ of alkali oxide in alkali borate melt from 100 to 70 BeF_2 mol %.

The interaction energy of polar groups, i.e. $>B\text{-}O^{\delta-}Na^{\delta+}$, $\gtrless Ge\text{-}O^{\delta-}Na^{\delta+}$ or $\gtrless Be\text{-}F^{\delta-}Li^{\delta+}$ in respective solutions consists of the following three terms[74]

1) the energy required to polarize the surrounding solution around the ion pair, whose polarization is calculated from the dielectric constant of the

surrounding solution containing ion-pairs and electrons in mixture by the Onsager's equation

2) the interaction energy between the ion pair and the reaction field from the polarized surrounding solution

3) the energy required to induce the electronic polarization of the ion pair by the reaction field.

The total interaction energy is given by

$$-\frac{p_{LiF}(R_{LiF} - R^{o}_{LiF})}{2}.$$

Where R^{o}_{LiF} and R_{LiF} are reaction fields in pure LiF and in LiF-BeF_2 mixture, respectively. p_{LiF} is dipole moment of LiF in vacuum. Permanent dipole moment of BeF_2 is neglected. The total interaction energy is rewritten as follows,

$$E_{dip} = \left\{\frac{3(P_A - P_B)N_0}{2(P_A\phi_A + P_B\phi_B)+3}\right\}\frac{X_A\phi_B r_A p_A^2}{v_A(2P_A+3)}$$

$$P_i = \frac{6\pi LN}{v_i}\left\{r_i\alpha_i + \frac{(r_i p_i)^2}{3KT}\right\}$$

$$r_i = \left(\frac{2\epsilon + 1}{2\epsilon + n_i^2}\right)\left(\frac{n_i^2 + 2}{3}\right)$$

where ϵ is the dielectric constant of $LiF-BeF_2$ mixture, n_i is the index of refraction, X_i is the mole fraction of species i, v_i is the partial volume, α_i is the electronic polarizability, N is the Avogadro number. The detailed explanation is given elsewhere[71,74].

The calculated energy is given in Figure 29, where dipole moment of 6.33 debye after Redington[75] and partial volume data by Cantor et al.[76] were used. Though the calculated energy is formally the integral free energy of the dipole-dipole interaction, such a large positive free energy suggests the dipole-dipole interaction can actually contribute to the positive enthalpies in $LiF-BeF_2$ obtained experimentally, which is shown in Figure 28. On the other hand the heat of mixting of $KF-BeF_2$ and $RbF-BeF_2$ system by Kleppa et al.[31] show the minimum of the enthalpy at 66.7 mol % KF or RbF definitly and partial enthalpies of KF and RbF decrease steeply from high alkali fluoride concentration at this composition. This means these mixtures can be explained by lattice model which have firstly proposed in oxide mixtures by Yokokawa et al.[24] The enthalpy change for net-work modification,

$$\rightarrow Be\text{-}F\text{-}Be\leftarrow + KF \rightleftharpoons BeF + \rightarrow BeF^- + 2K^+$$

is considered constant over all composition range.

According to this consideration, even in LiF-BeF_2 system, the similar negative integral enthalpy can be considered for net-work modification. In this system, positive integral enthalpy, ΔH_{LiF}(dip) for dipole-dipole interaction, and negative ΔH_{LiF}(net-work) which arises from net-work modification can reproduce the peculiar behavior of integral as well as partial molar enthalpies qualitatively. These behavior of enthalpies of LiF-BeF_2 system especially in high BeF_2 content, remind us the behaviors of alkali borate or alkali germanate melt. The present author considers the dipole-dipole interaction energy determines the decrease of $\Delta\bar{H}_{A_2O}$ from 100 to 90 mol % B_2O_3, GeO_2 and determines the positive deviation of activity of SiO_2 in alkali silicate melt[77] also from the view point of thermostatics.

In alkali borate glasses, some of boron atoms are known to be four-foldly coordinated[57] by oxygen atoms. It is reported by Krogh-Moe[78] that in alkali borate glasses the saturation of four-fold coordination occurs at about 40 mol % A_2O and the coordination disappears at about 50 mol %. On the other hand, $\Delta\bar{H}_{Li_2O}$ and $\Delta\bar{H}_{Na_2O}$ become nearly constant around the meta-borate composition as is seen in Figure 24. Therefore, we think that the large increase of $\Delta\bar{H}_{A_2O}$ up to the meta-borate concentration includes, in addition to the heat of the net-work modification, the heat effect due to

the relative decrease of the four-foldly coordinated B atoms per added A_2O.

Figure 26 shows a very large decrease of $\Delta\overline{S}_{A_2O}$ compared with the ideal configurational entropy change in A_2O concentration from zero to 10 mol %. We think the dipole-dipole interaction, varying with the inter-pair distance, contributes to the entropy through the ordering. On the other hand, the four-fold coordination affect the entropy oppositely, since the coordination's effect to lower the entropy should be the highest in infinite dilution of A_2O and the effect becomes weaker gradually as A_2O concentration increases.

One may note a drastic increase in $\Delta\overline{S}_{A_2O}$ in the concentration region from 85 to 70 mol %, in Figure 26, which can be explained by the collapse both of the net-work and of the ordering with four-fold coordination which dominates below that range to infinite dilution of A_2O.

Finally we like to mention the basicity of molten oxides. Hitherto, many definitions of basicities have been proposed and used conventionally[79,80]. Here we consider that activity of B_2O_3 in Figure 23 is one of the most obvious representations of basicity where B_2O_3 can be the common measure in many oxide-boron oxide mixtures. The strength of metal oxides in B_2O_3 melts as a base is in the order $K_2O > Na_2O > Li_2O > Ag_2O > PbO$.

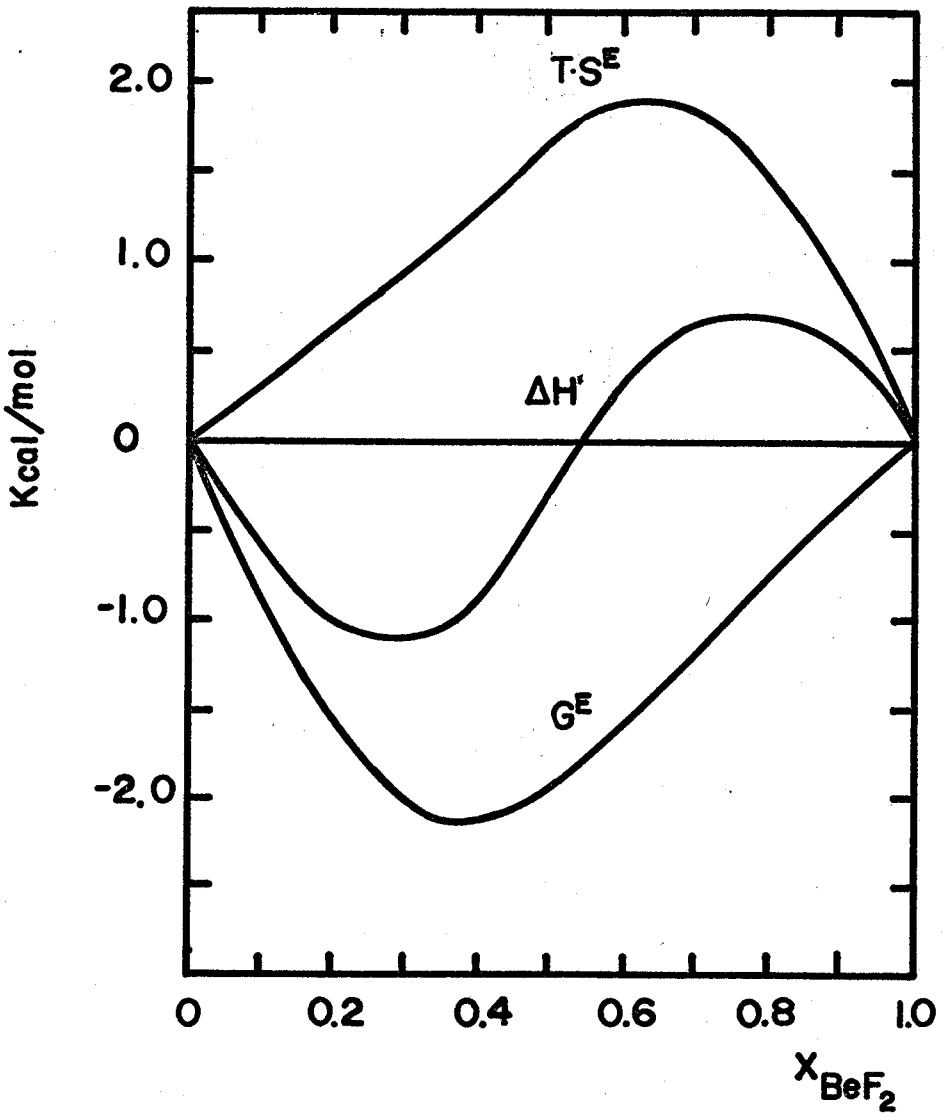

Figure 28. Liquid mixtures of $LiF-BeF_2$ at 862°C

Kleppa et al. Baes et al.

Figure 29. Excess free energy of mixing for $LiF-BeF_2$ mixture, obtained from dipole-dipole interaction.

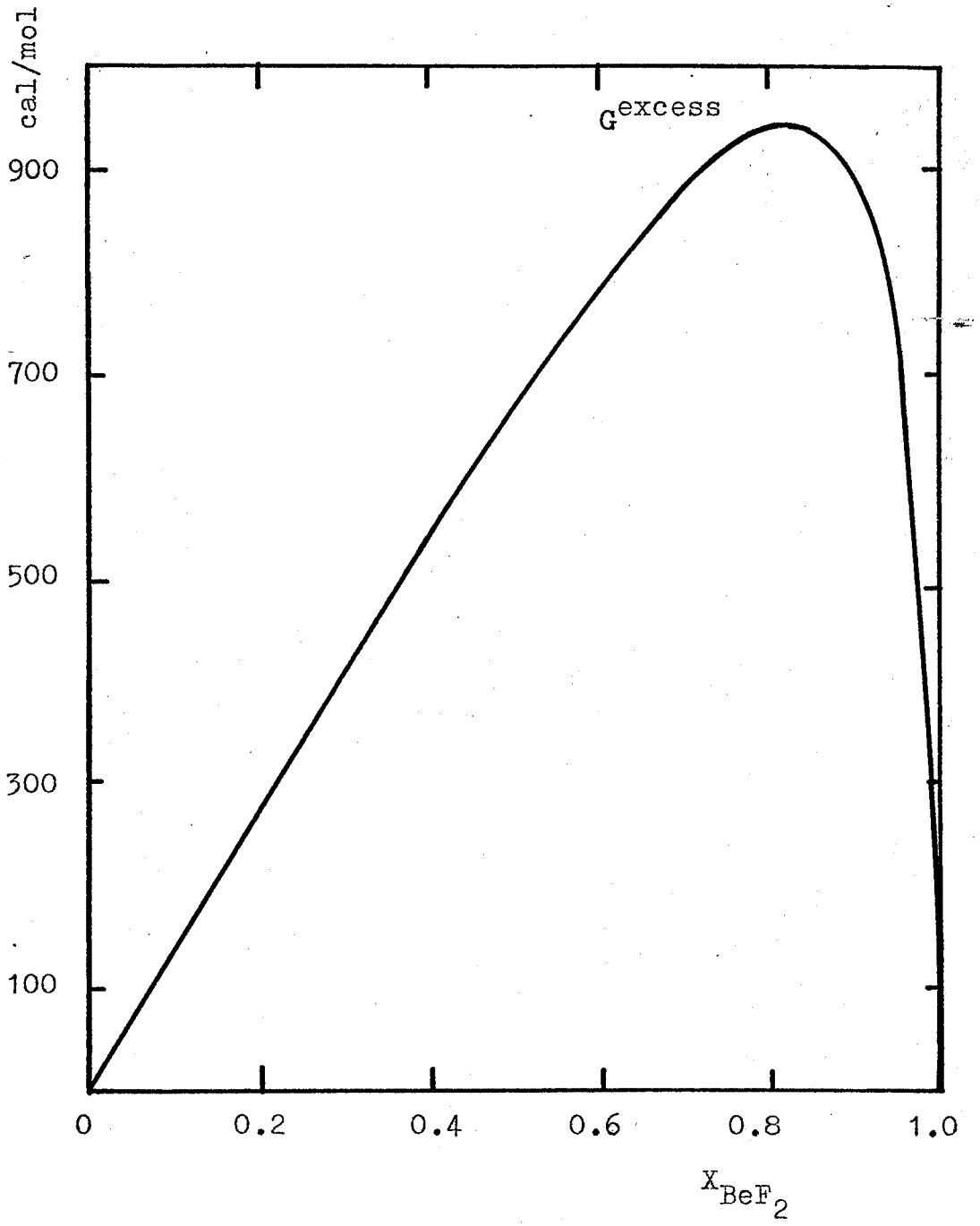

REFERENCES

1. Endell and Hellbrugge, Arch. Eisenhuttenw., 14, 307 (1941).
2. L. Shartsis, S. Spinner, and W. Capps, J. Amer. Ceram. Soc., 35, 155 (1952).
3. J. O'M. Bockris, J. D. Mackenzie and J. A. Kitchener, Trans. Faraday Soc., 51, 1734 (1955).
4. J. O'M. Bockris, J. A. Kitchener, S. Ignatowicz and J. W. Tomlinson, ibid., 48, 75 (1952).
5. L. Shartsis, W. Capps and S. Spinner, J. Amer. Ceram. Soc., 36, 319 (1953).
6. L. Shartsis, W. Capps and S. Spinner, ibid., 36, 35 (1953).
7. E. F. Riebling, J. Chem. Phys., 39, 1889 (1963).
8. E. F. Riebling and S. D. Gabelnick, J. Electrochem. Soc., 112, 822 (1965).
9. B. E. Warren and J. Biscoe, J. Amer. Ceram. Soc., 21, 259 (1938).
10. T. B. King and S. Ramachandran, The Phy. Chem. Steelmaking, Tech Press MIT, (1958) pp 125.
11. R. Schuhman and P. J. Ensio, Trans. A.I.M.E., 191, 401 (1951).
12. H. Kojima and C. R. Masson, Canadian J. Chem., 47, 4221 (1969).
13. F. D. Richardson, Trans. Faraday Soc., 52, 1312 (1956).

14. F. C. Kracek, J. Amer. Chem. Soc., 52, 1436 (1930).
15. The Physical Chemistry of Melts, by the Nuffield Research Group, Inst. Min. Met., London (1953).
16. G. Willis and F. Hennessy, Trans. AIME , 197, 1367 (1953).
17. T. Maekawa, T. Yokokawa and K. Niwa, Bull. Chem. Soc. Jap., 42, 677 (1969).
18. H. Franz, Glaschechn. Ber., 38, 54 (1965).
19. C. E. Adams and J. T. Quan, J. Phys. Chem., 70, 331 (1966).
20. A. Büchler and J. B. Berkowitz-Mattuck, J. Chem. Phys., 39, 286 (1963).
21. G. W. Toop and C. S. Samis, Trans. Met. Soc. AIME, 224, 878 (1962).
22. C. R. Masson, Proc. Roy. Soc., A 287, 201 (1965).
23. S. G. Whiteway, I. B. Smith and C. R. Masson, Can. J. Chem., 48, 33 (1970).
24. T. Yokokawa and K. Niwa, Trans. Jap. Inst. Met., 10, 3 (1969).
25. T. Yokokawa and K. Niwa, ibid., 10, 81 (1969).
26. M. L. Kapoor and M. G. Frohberg, Arch. Eisenhutt., 41, 1035 (1970).
27. T. Yokokawa and O. J. Kleppa, Inorg. Chem., 4, 1806 (1965).
28. A. Navrotsky and O. J. Kleppa, J. Inorg. Nucl. Chem., 29, 2701 (1967).

29. T. Østvold and O. J. Kleppa, Inorg. Chem., 9, 1395 (1970).
30. T. Østvold and O. J. Kleppa, ibid., 8, 78 (1969).
31. J. L. Holm and O. J. Kleppa, ibid., 8, 207 (1969).
32. P. Csaki and A. Dietzel, Glastechn. Ber., 18, 33 (1940).
33. W. Stegmaier and A. Dietzel, ibid., 18, 353 (1940).
34. H. Flood, T. Førland and K. Motzfeldt, Acta. Chem. Scand., 6, 257 (1952).
35. K. Kiukkola and C. Wagner, J. Electrochem. Soc., 104, 379 (1957).
36. S. Sato, T. Yokokawa, H. Kita and K. Niwa, J. Electrochem. Soc., 119, 1524 (1972).
37. S. Sato and T. Yokokawa, Trans. Jap. Inst. Met., 16, 441 (1975).
38. M. Itoh, S. Sato and T. Yokokawa, J. Chem. Thermodynamics (in press).
39. H. Schmalzried, Z. Elektrochemie, 66, 572 (1962).
40. T. A. Ramanarayanan and R. A. Rapp, Met. Trans., 3, 3239 (1972).
41. J. D. Mackenzie, Chem. Rev., 56, 455 (1956).
42. M. L. Pearce, J. Amer. Ceram. Soc., 48, 175 (1965).
43. A. Gosh and T. B. King, Trans. AIME, 245, 145 (1969).
44. M. Kawakami and K. Goto, TETSU-TO-HAGANE, 59, 14 (1973).

45. Jeffes, J. H. E., Sridhar, R. In Electromotive Force Measurements in High-Temperature Systems, C. B. Alcock edted, Inst. Min. Met., London (1968).
46. see for example, Modern aspect of electrochemistry, ed. by J. O'M. Bockris, (1954) p 261.
47. I. D. Shah and N. A. D. Parlee, Trans. Met. Soc. AIME, 2239, 763 (1967).
48. J. Osterwald and G. Schwarzlose, Z. Phys. Chem. N. F., 62, 763 (1968).
49. K. Suzuki and K. Mori, TETSU-TO-HAGANE, 57, 51 (1971).
50. S. Honma, N. Sano and Y. Matsushita, Met. Trans., 2, 1494 (1971).
51. H. Rickert and A. A. El Miligy, Z. Metallk., 59, 635 (1968)
52. J. Crank, The Mathematics of Diffusion, p 45, Oxford University Press, London (1956).
53. S. Otsuka, I. Katayama and Z. Kozuka, Trans. Jap. Inst. Met., 12, 442 (1971).
54. C. E. Vallet and J. Braunstein, J. Amer. Ceram. Soc., 58, 209 (1975).
55. S. Kohsaka, S. Sato and T. Yokokawa, (to be published).
56. Phase Diagrams for Ceramists edited, E. M. Levin, C. R. Robbins and H. F. Mcmurdie, The Amer. Ceram. Soc., (1964).
57. P. J. Bray and A. H. Silver, in Modern Aspect of Vitreous State ed., Mackenzie Butterworths, London (1960).

58. E. Amrhein, Glastechn. Ber., 36, 425 (1963).

59. B. E. Conway, in Physical Chemistry an Advanced Treatise Vol. IX A/ Electrochemistry ed. H. Eyring, Academic Press New York (1970).

60. T. Førland, in Fused Salts, ed. B. R. Sundheim, p 157, Mcgraw-Hill Book Company, New York (1964).

61. H. Kodama, Y. Kimura, T. Yokokawa and K. Niwa, Bull. Chem. Soc. Jap., 42, 681 (1969).

62. H. Kodama, T. Yokokawa and K. Niwa, Bull. Chem. Soc. Jap., 45, 776 (1972).

63. J. D. Mackenzie, J. Phys. Chem., 63, 1875 (1959).

64. G. Treiber and K. Tödheide, Ber. Bunsenges. Physik. Chem., 77, 540 (1973).

65. B. Bardoll and K. Tödheide, ibid., 79, 490 (1975).

66. J. O'M. Bockris, E. H. Crook, H. Bloom and N. E. Richards, Proc. Roy. Soc., (London) A 255, 558 (1960).

67. M. Buback and E. U. Franck, Ber. Bunsenges. Physik. Chem., 77, 1074 (1973).

68. G. Treiber and K. Tödheide, ibid., 77, 1079 (1973).

69. J. O'M. Bockris, in Fused Salts, ed. B. R. Sundheim, p 19, Mcgraw-Hill Book Company, New York (1964).

70. K. Goto, Nippon Kinzoku Gakkai Kaiho, 10, 745 (1973).

71. R. W. Haskell, J. Phys. Chem., 73, 2916 (1969).

72. J. L. Holm, Docter Thesis,

73. B. F. Hitch and C. F. Baes, Jr, Inorg. Chem., 8, 201 (1969).

74. H. Fröhlich, Theory of Dielectrics, Oxford at the Clarendon Press (1958).
75. R. L. Redington, J. Chem. Phys., 44, 1238 (1966).
76. S. Cantor, W. T. Ward and C. T. Moynihau, J. Chem. Phys., 50, 2874 (1969).
77. F. D. Richardson, Physical Chemistry of Melts in Metallurgy Academic Press (London), (1973).
78. J. Krogh-Moe, Phys. Chem. Glass., 3, 1 (1962).
79. N. Masuko, J. Electrochem. Soc. Japan, 35, 508 (1967).
80. M. G. Frohberg, Stahl u. Eisen, 91, 182 (1971).
81. H. C. Ko and O. J. Kleppa, Inorg. Chem., 10, 771 (1971).
82. E. A. Guggenheim, Mixtures, Oxford Press, (1952).